Critical end point and universality class of neutron $^3P_2$ superfluids in neutron stars

Takeshi Mizushima,[1,*] Shigehiro Yasui,[2,†] and Muneto Nitta[2,‡]
[1]*Department of Materials Engineering Science, Osaka University, Toyonaka, Osaka 560-8531, Japan*
[2]*Department of Physics & Research and Education Center for Natural Sciences, Keio University, Hiyoshi 4-1-1, Yokohama, Kanagawa 223-8521, Japan*

(Received 23 September 2019; revised manuscript received 28 December 2019; accepted 20 January 2020; published 24 February 2020)

We study the thermodynamics and critical behavior of neutron $^3P_2$ superfluids in the inner cores of neutron stars. $^3P_2$ superfluids offer a rich phase diagram including uniaxial/biaxial nematic phases, the ferromagnetic phase, and the cyclic phase. Using the Bogoliubov–de Gennes equation as in superfluid Fermi liquid theory, we show that a strong (weak) magnetic field drives the first-order (second-order) transition from the dihedral-two biaxial nematic phase to the dihedral-four biaxial nematic phase at low (high) temperatures and their phase boundaries are divided by the critical end point (CEP). We demonstrate that the set of critical exponents at the CEP satisfies the Rushbrooke, Griffiths, and Widom equalities, indicating a different universality class. At the CEP, the $^3P_2$ superfluid exhibits critical behavior with nontrivial critical exponents, indicating an alternative universality class. Furthermore, we find that the Ginzburg-Landau (GL) equation up to the eighth-order expansion satisfies three equalities and properly captures the physics of the CEP. This implies that the GL theory can provide a tractable way for understanding critical phenomena which may be realized in the dense core of realistic magnetars.

DOI: 10.1103/PhysRevResearch.2.013194

I. INTRODUCTION

A neutron star is a compact star which is composed almost entirely of neutrons under extreme conditions such as high density, rapid rotation, and a strong magnetic field (see Refs. [1,2] for recent reviews). The most recent discoveries include observations of massive neutron stars whose masses are almost twice as large as the solar mass [3,4] and observation of gravitational waves from a binary neutron star merger [5]. In the inner structure, neutron superfluidity and proton superconductivity are key ingredients for understanding the evolution of neutron stars (see Refs. [6–8] for recent reviews). As the superfluid and superconducting components reorganize low-lying elementary excitations, their presence profoundly affects neutrino emissivities and specific heats and can explain the long relaxation time observed in the sudden speed-up events of neutron stars [9–11] and the enhancement of neutrino emission at the onset of superfluid transition [12–17]. Sudden changes of spin periods observed in pulsars (pulsar glitches) may also be explained by the existence of superfluid components with quantized vortices [18,19].

We notice that the $^1S_0$ channel, which is attractive at low density, becomes repulsive in the high-density regime.[1] Instead, the neutron $^3P_2$ superfluids can be realized in the high-density regime $\rho \gtrsim 10^{14}\mathrm{g/cm}^3$ (ρ is the density of neutrons), where the $^3P_2$ interaction stems from a strong spin-orbit force between two nucleons [22–40].[2] Hence, the neutron $^3P_2$ superfluids are expected to be realized in the inner cores of neutron stars. Furthermore, the neutron $^3P_2$ superfluids have tolerance against the strong magnetic field, such as 10^{15}–10^{18} G in magnetars, because the spin-triplet pairing is not broken through the spin–magnetic-field interaction by Zeeman effects.[3] It has recently been proposed that the observation of the rapid cooling of the neutron star in Cassiopeia A may be explained by enhanced neutrino emissivities due to the formation and dissociation of neutron Cooper pairs in the $^3P_2$ channel, which is a short-range attraction in the total

*mizushima@mp.es.osaka-u.ac.jp
†yasuis@keio.jp
‡nitta@phys-h.keio.ac.jp

[1]In the literature, the $^1S_0$ superfluidity at low density was proposed in Ref. [20]. However, it was pointed out in Ref. [21] that this channel becomes repulsive due to the strong core repulsion at higher densities.

[2]We note that the interactions in the $^3P_0$ and $^3P_1$ channels are repulsive at high density, and hence they are irrelevant to the formation of the superfluidity [41].

[3]The origin of the strong magnetic fields in neutron stars or in magnetars has been studied in several types of mechanisms such as spin-dependent interactions [42–45], pion domain walls [46,47], and spin polarizations in the quark matter in the neutron star core [48–50]. However, this problem is not settled yet. Recently, a negative result for the generation of strong magnetic fields was reported in a study based on the nuclear many-body calculations [51].

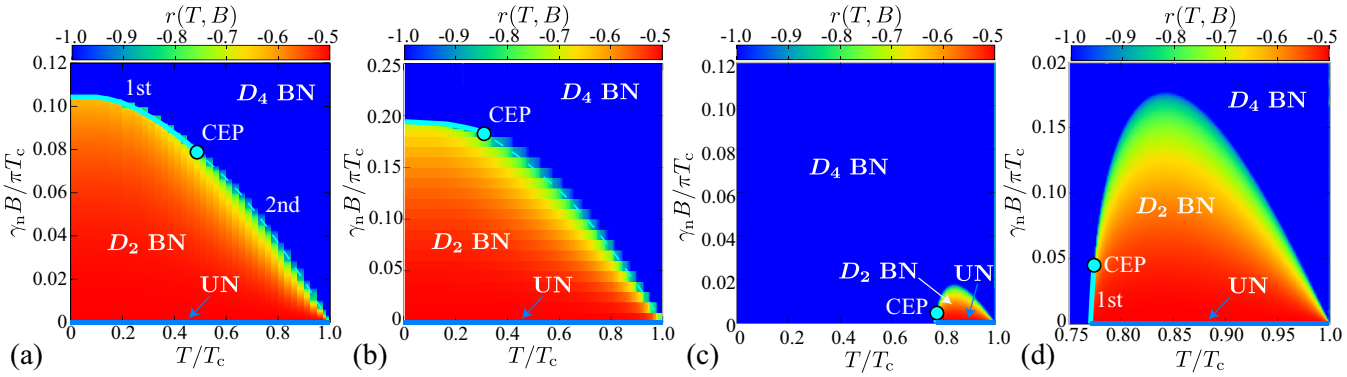

FIG. 1. Phase diagram of $^3P_2$ superfluids under a magnetic field computed with the superfluid Fermi liquid theory for the Fermi liquid parameter (a) $G_0^{(n)} = -0.7$ and (b) $G_0^{(n)} = -0.4$. The thick solid (thin dashed) curve is the first-order (second-order)phase boundary and CEP denotes the critical end points. (c) and (d) Phase diagram for $G_0^{(n)} = -0.75$ computed from the GL theory with the eighth-order expansion. In the GL theory, the critical end point is given by $T_{CEP}/T_c = 0.774\,597$ and $\gamma_n B_{CEP}/\pi T_c = 0.004\,465$. The colormap in (a)–(d) represents the nematic order parameter $r(T, B)$.

angular momentum $J = 2$ [15–17] (see also Refs. [52–54]). Theoretically, neutron $^3P_2$ superfluids provide a fertile ground for exploring exotic superfluidity. The superfluid states with $J = 2$ are classified into several phases: nematic, cyclic, and ferromagnetic phases [27,28,55–60]. The nematic phase is further divided into the uniaxial nematic (UN) phase and the dihedral-two and dihedral-four biaxial nematic (D_2-BN and D_4-BN) phases. All these phases are accompanied by topologically protected Bogoliubov quasiparticles. The nematic phase is a prototype of class-DIII topological superconductors and a cluster of Majorana fermions [61]. The other phases are nonunitary states with broken time-reversal symmetry and promising platforms to host Weyl superfluidity [61,62]. In addition to such exotic fermions, the $^3P_2$ order parameters also bring about rich bosonic excitations [63–75], which might be relevant to the cooling process by neutrino emission,[4] as well as exotic topological defects, including spontaneously magnetized vortices [27,56,57,59] and vortices with Majorana fermions [77], solitonic excitations on a vortex [78], and half-quantized non-Abelian vortices [60], domain walls [79], and surface topological defects (boojums) on the boundary of $^3P_2$ superfluids [80]. Those states share common properties in condensed-matter systems such as D-wave superconductors [81], P-wave superfluidity in ^{3}He liquid [82–84], chiral P-wave superconductivity, e.g., in Sr_2RuO_4 [85,86] and U-based ferromagnetic superconductors [87], and spin-2 Bose-Einstein condensates [88].

The neutron $^3P_2$ superfluidity can be described by the Fermi liquid theory which is composed of the set of self-consistent equations based on the Luttinger-Ward thermodynamic functional. Microscopically, the most fundamental equation of the neutron $^3P_2$ superfluidity is provided by the Bogoliubov–de Gennes (BdG) equation where the order parameter, i.e., gap function, should be solved self-consistently with the wave functions of the gapped neutrons [22–25,30,32–40]. The BdG equation was successfully applied to study the topological properties of the neutron $^3P_2$ superfluidity [61]. The phase diagram with respect to the magnetic field and temperature was obtained in Ref. [61], where the first- and second-order phase transitions between the D_2-BN and D_4-BN phases are present and these transitions meet at a critical end point (CEP), as shown in Figs. 1(a) and 1(b).[5] The existence of the CEP is certainly important for transport coefficients and equations of state of neutron matter when neutron stars are cooled down.

Around the transition temperature from the normal phase to the superfluid phase, the Ginzburg-Landau (GL) theory can be induced by the systematic expansion of the functional with respect to the order parameter field and the magnetic field [27,28,55–60,80,89–91]. Unlike the ordinary cases, the GL expansion up to the fourth order in terms of the order parameter cannot determine the unique ground state, but there exists a continuous degeneracy among the UN, D_2-BN, and D_4-BN phases.[6] The GL expansion up to the sixth order determines the unique ground state [59], but it is stable only locally and an instability exists for a large value of the order parameter. Recently, in order to solve this problem, the GL equation up to the eighth-order term in the condensates was obtained [91], in which it was shown that the eighth-order term ensures the global stability with respect to the variation of the order parameter in the ground state. As a by-product, it was also found that the phase diagram in the expansion up to the eighth order possesses the CEP as shown in Fig. 1(c), in contrast to the GL equation up to the sixth order in which no CEP exists, although the positions of the CEPs in the BdG and GL formalisms are rather different, as shown in Fig. 1(d).

In this paper we study the critical exponents at the CEP in the BdG equation and in the GL equation. Under the scaling

[4]The cooling process is related not only to low-energy excitations but also to quantum vortices [76].

[5]See Eqs. (30) and (34) for the definitions of $G^{(n)}$.

[6]We notice that, at the fourth order, an SO(5) symmetry happens to exist as an extended symmetry in the potential term, which is absent in the original Hamiltonian. In this case, the spontaneous breaking eventually generates a quasi-Nambu-Goldstone mode, which should be irrelevant to the excitations in the true ground state [92]. This is nothing but the origin of the continuous degeneracy.

hypothesis, a set of critical exponents[7] $(\alpha, \beta, \gamma, \delta)$ at the CEP should satisfy the the universal relations, i.e., the Rushbrooke, Griffiths, and Widom equalities

$$\alpha + 2\beta + \gamma = 2 \quad \text{(Rushbrooke)}, \tag{1}$$

$$\alpha + \beta(1+\delta) = 2 \quad \text{(Griffiths)}, \tag{2}$$

$$-\frac{\gamma}{\beta} + \delta = 1 \quad \text{(Widom)}. \tag{3}$$

In both cases of the BdG equation and the GL equation, we extract the critical behavior of neutron $^3P_2$ superfluids by directly computing all the critical exponents at the CEP. We demonstrate that the CEP in the GL approach properly captures the critical phenomena in the BdG equation and the exponents satisfy all three equalities reasonably in both the BdG and GL equations within a numerical error. We find that the $^3P_2$ superfluid at the CEP exhibits critical behavior with nontrivial critical exponents in such a manner that the exponents associated with the critical behaviors of the specific heat and magnetization exhibit $\alpha \sim 0.6$ and $\gamma \sim 0.5$. In particular, the exponent $\gamma < 1$ is unique and essentially different from $\gamma \geqslant 1$ in ordinary universality classes [93,94], except for a few models, e.g., O(n) models with $n < 0$ [95] and the tricritical Ising model coupled to massless Dirac fermions [96]. This indicates that the CEP in neutron $^3P_2$ superfluids belongs to a different universality class.

The organization of this paper is as follows. In Sec. II we present the superfluid Fermi liquid theory, where the self-consistent equations for the gap functions and Fermi liquid corrections are described in detail. This theory is based on the quasiclassical approximation which is relevant to $^3P_2$ superfluids of neutrons. Based on the theory, we show that the phase diagram of $^3P_2$ superfluids under strong magnetic fields has the CEP and compute the critical exponents, indicating a different universality class. Furthermore, in Sec. III we present the GL theory up to the eighth-order expansion to examine the critical phenomena at the CEP, showing that the critical exponents in the GL theory coincide with those in the BdG theory within a certain accuracy. Section IV is devoted to a summary and discussion.

II. SUPERFLUID FERMI LIQUID THEORY

A. General formalism

Here we start with the Hamiltonian for neutrons interacting through the potential $\mathcal{V}^{c,d}_{a,b}$,

$$\mathcal{H} = \int d\boldsymbol{r}\, \psi^\dagger_a(\boldsymbol{r})\xi_{ab}(-i\nabla)\psi_b(\boldsymbol{r}) + \frac{1}{2}\int d\boldsymbol{r}_1 \int d\boldsymbol{r}_2 \mathcal{V}^{c,d}_{a,b}(\boldsymbol{r}_{12})\psi^\dagger_a(\boldsymbol{r}_1)\psi^\dagger_b(\boldsymbol{r}_2)\psi_c(\boldsymbol{r}_2)\psi_d(\boldsymbol{r}_1), \tag{4}$$

where $\boldsymbol{r}_{12} \equiv \boldsymbol{r}_1 - \boldsymbol{r}_2$ denotes the relative coordinate and ψ_a and $\psi^\dagger_a$ ($a = \uparrow, \downarrow$ for spins) denote the fermionic field operators. The single-particle energy for a neutron under a magnetic field $\boldsymbol{B}$ is given by

$$\xi(\boldsymbol{k}) = \xi_0(\boldsymbol{k}) - \tfrac{1}{2}\gamma_n \boldsymbol{\sigma}\cdot\boldsymbol{B}, \tag{5}$$

with $\xi_0(\boldsymbol{k}) = \boldsymbol{k}^2/2m - \mu$ for the neutron mass m and the chemical potential μ. Here $\gamma_n = 1.2 \times 10^{-13}$ MeV/T is the gyromagnetic ratio for a neutron[8] and $\boldsymbol{\sigma} = (\sigma_1, \sigma_2, \sigma_3)$ denotes the Pauli matrices in the spin space. In Eq. (4), $\mathcal{V}^{c,d}_{a,b}(\boldsymbol{r}_{12})$ contains microscopic information on neutron-neutron interaction potentials. The repeated latin and greek indices imply the sum over the spin degrees of freedom and the three-dimensional spatial component (x, y, z), respectively. In this paper we set $\hbar = k_B = 1$.

Let us define the Nambu-Gor'kov (NG) Green's function in terms of a grand ensemble average of the fermion-field operators in the Nambu space, $\Psi \equiv (\psi_\uparrow, \psi_\downarrow, \psi^\dagger_\uparrow, \psi^\dagger_\downarrow)^{\rm tr}$, as $G(x_1, x_2) = -\langle \mathrm{T}_\tau \Psi(x_1)\Psi^\dagger(x_2)\rangle$, where $x_i \equiv (\boldsymbol{r}_i, \tau_i)$ with the three-dimensional space position $\boldsymbol{r}_i$ and the imaginary time τ_i for the neutron $i = 1, 2$. Here $a^{\rm tr}$ denotes the transpose of the matrix a. In this paper we consider translationally invariant neutron matter and transform the space-time position x to momentum $\boldsymbol{p}$ and Matsubara frequency $\varepsilon_n = (2n+1)\pi T$ ($n = 0, \pm1, \pm2, \ldots$): $x \to (\boldsymbol{p}, \varepsilon_n)$. The self-consistent formalism is derived from the Luttinger-Ward thermodynamic functional, which is given in terms of the full NG Green's function G and the self-energy Σ as

$$\Omega[G, \Sigma] = -\tfrac{1}{2}\mathrm{Sp}\{\Sigma G + \ln\left(-G_0^{-1} + V_{\rm ext} + \Sigma\right)\} + \Phi[G], \tag{6}$$

where

$$\mathrm{Sp}\cdots \equiv T\sum_n \int \frac{d^3p}{(2\pi)^3}\mathrm{Tr}\cdots, \tag{7}$$

with the trace (Tr) taken over the spin space and the NG (particle-hole) space. The inverse propagator for free fermions is given by $G_0^{-1}(\boldsymbol{p}, \varepsilon_n) = [i\varepsilon_n - \xi_0(\boldsymbol{p})\tau_3]\delta(x - x')$ and $V_{\rm ext}$ is an external field including a magnetic Zeeman term in Eq. (5). Here we use $\boldsymbol{\tau} = (\tau_1, \tau_2, \tau_3)$ to denote the matrices in the NG space. The Green's function and the self-energy are related to the functional $\Phi[G]$ by the stationary conditions with respect to the Green's function $\delta\Omega/\delta G^{\rm tr} = 0$ and the self-energy $\delta\Omega/\delta\Sigma^{\rm tr} = 0$. The former is recast into the definition of the self-energy in terms of the functional derivative

$$\Sigma[G] = 2\frac{\delta\Phi[G]}{\delta G^{\rm tr}}. \tag{8}$$

The Dyson equation for the full Green's function is obtained from the latter stationary condition as

$$G^{-1} = G_0^{-1} - V_{\rm ext} - \Sigma[G]. \tag{9}$$

The set of equations (6)–(9) provides a starting point for deriving the quasiclassical Fermi liquid theory for $^3P_2$ superfluids.

[7] See Eqs. (57)–(59) for the definitions of $(\alpha, \beta, \gamma, \delta)$.

[8] Note the unit conversion 1 T $= 10^4$ G for the strength of a magnetic field.

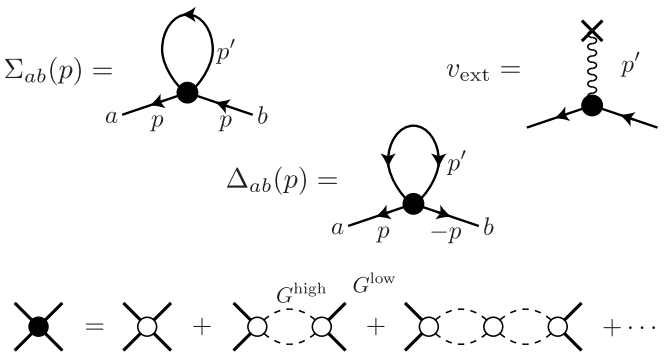

FIG. 2. Leading-order contributions to quasiclassical self-energies. Closed circles, which couple to low-energy propagators (solid lines), show the particle-hole and particle-particle vertices $\Gamma^{\rm ph}$ and $\Gamma^{\rm pp}$ that sum all orders of the bare interaction (open circles) and high-energy intermediate states $G^{\rm high}$ (dashed lines). The particle-hole and particle-particle vertices determine the leading-order quasiparticle self-energy and pair potential, respectively.

B. Quasiclassical approximation

In general, the quasiclassical approximation provides a powerful tool for describing phenomena when the characteristic lengths are much greater than the Fermi wavelength $\lambda_{\rm F} \sim 2\pi/p_{\rm F}$ (with $p_{\rm F}$ the Fermi momentum) and characteristic frequencies are much smaller than the Fermi energy $\omega \ll \varepsilon_{\rm F}/\hbar$ (with $\varepsilon_{\rm F}$ the Fermi energy) [97,98]. The typical scales in the superfluid state of ^{3}He and superconducting states are the coherence length $\xi_{\rm c} \equiv \hbar v_{\rm F}/2\pi k_{\rm B} T_{\rm c}$ and the excitation gap $\Delta_0 \sim k_{\rm B} T_{\rm c}$. The quasiclassical theory uses the fact that all relevant parameters, such as temperature T and external potentials V, are very small relative to the atomic scales which are given by Fermi temperature $T_{\rm F}$, Fermi energy $\varepsilon_{\rm F}$, and Fermi momentum $p_{\rm F}$. This difference in scales allows one to perform an asymptotic expansion of full many-body propagators in small parameters $T/T_{\rm F}$ and $|V|/\varepsilon_{\rm F}$ and it leads eventually to integrating out all quantities that vary on the atomic scales.

A key feature of the quasiclassical approximation is that G is sharply peaked at the Fermi surface and depends weakly on energies far away from it. We use this assumption to split the propagator into low- and high-energy parts $G = G^{\rm low} + G^{\rm high}$, where $G^{\rm low}(\boldsymbol{p}, \varepsilon_n) = G(\boldsymbol{p}, \varepsilon_n)$ for $|\varepsilon| < \varepsilon_{\rm c}$ and $G^{\rm low}(\boldsymbol{p}, \varepsilon_n) = 0$ for $|\varepsilon| > \varepsilon_{\rm c}$. The cutoff energy $\varepsilon_{\rm c}$ is taken to be $\varepsilon_{\rm c} \ll \varepsilon_{\rm F}$. As shown in Fig. 2, we introduce the renormalized vertices (closed circles) that sum an infinite set of diagrams composed of the high-energy part of the propagator and the bare vertices (open circles). The low-energy part of the propagator obeys the Dyson equation

$$G^{\rm low}(\boldsymbol{p}, \varepsilon_n) = G_0^{\rm low}(\boldsymbol{p}, \varepsilon_n) + G_0^{\rm low}(\boldsymbol{p}, \varepsilon_n)\Sigma(\boldsymbol{p}, \varepsilon_n)G^{\rm low}(\boldsymbol{p}, \varepsilon_n), \tag{10}$$

where $G_0^{\rm low}$ denotes the low-energy part for the free propagator. This equation will play an important role in the following discussion.

For the convenience of the analysis, we define the quasiclassical propagator for the low-energy part $\mathfrak{g}(\boldsymbol{p}_{\rm F}, \varepsilon_n)$ as an integral over a shell $|\boldsymbol{v}_{\rm F} \cdot (\boldsymbol{p} - \boldsymbol{p}_{\rm F})|$ in momentum space near the Fermi surface

$$\mathfrak{g}(\boldsymbol{p}_{\rm F}, \varepsilon_n) = \frac{1}{a}\int_{-\varepsilon_{\rm c}}^{\varepsilon_{\rm c}} d\xi_p \tau_3 G^{\rm low}(\boldsymbol{p}, \epsilon_n), \tag{11}$$

where $\xi_p = \boldsymbol{v}_{\rm F} \cdot (\boldsymbol{p} - \boldsymbol{p}_{\rm F})$, with $\boldsymbol{v}_{\rm F} = \boldsymbol{v}(\boldsymbol{p}_{\rm F})$ and $\boldsymbol{v}(\boldsymbol{p}) = \partial\xi(\boldsymbol{p})/\partial\boldsymbol{p}$ the Fermi velocity. The propagator is normalized by dividing by the weight of the quasiparticle pole in the spectral function a. The quasiclassical propagator matrix is parametrized as

$$\mathfrak{g} = \begin{pmatrix} g_0 + \boldsymbol{g}\cdot\boldsymbol{\sigma} & i\sigma_y f_0 + i\boldsymbol{\sigma}\cdot\boldsymbol{f}\sigma_y \\ i\sigma_y \bar{f}_0 + i\sigma_y\boldsymbol{\sigma}\cdot\bar{\boldsymbol{f}} & \bar{g}_0 + \bar{\boldsymbol{g}}\cdot\boldsymbol{\sigma}^{\rm tr} \end{pmatrix}, \tag{12}$$

where f_0 and $\boldsymbol{f}$ represent the spin-singlet and spin-triplet components of anomalous propagators and g_0 and $\boldsymbol{g}$ represent the spin-singlet and spin-triplet components of normal propagators. The Matsubara propagators maintain the following sets of symmetry relations in the NG space:

$$[\mathfrak{g}(\boldsymbol{p}_{\rm F}, \varepsilon_n)]^\dagger = \tau_3 \mathfrak{g}(\boldsymbol{p}_{\rm F}, -\varepsilon_n)\tau_3, \tag{13}$$

$$[\mathfrak{g}(\boldsymbol{p}_{\rm F}, \varepsilon_n)]^{\rm tr} = \tau_2 \mathfrak{g}(-\boldsymbol{p}_{\rm F}, -\varepsilon_n)\tau_2. \tag{14}$$

To convert the Dyson equation (9) to a transportlike equation, we first perform the left-right subtraction trick for quasiclassical propagators, i.e.,

$$G^{-1}\tau_3 \otimes \tau_3 G - \tau_3 G G^{-1}\tau_3 = 0. \tag{15}$$

The inverse Green's function for free fermions G_0^{-1} is replaced with $a^{-1}[\varepsilon - \xi(\boldsymbol{p})\tau_3]$ if we include renormalization of the normal propagator by the zeroth-order self-energy in the small parameter, i.e., $T_{\rm c}/T_{\rm F} \ll 1$ or $\varepsilon_{\rm c}/\varepsilon_{\rm F} \ll 1$. We recall that a is the weight of the quasiparticle pole in the spectral function. The kinetic equation is then reduced to

$$[\varepsilon\tau_3 - aV_{\rm ext}\tau_3 - a\Sigma\tau_3, \tau_3 G] = 0. \tag{16}$$

An important property of the self-energies is their weak dependence on momentum. We suppose that their characteristic momentum scale is set by the Fermi momentum $\boldsymbol{p}_{\rm F}$. For the quasiclassical renormalized perturbation, we can introduce $v_{\rm ext}$ and $\sigma_{\rm MF}$, which are related to an external potential $V_{\rm ext}$ and self-energy Σ taken at the Fermi level by

$$v_{\rm ext}(\boldsymbol{p}_{\rm F}) = aV_{\rm ext}(\boldsymbol{p})\tau_3, \quad \sigma_{\rm MF}(\boldsymbol{p}_{\rm F}) = a\Sigma(\boldsymbol{p})\tau_3, \tag{17}$$

respectively, with $\boldsymbol{p} \approx \boldsymbol{p}_{\rm F}$. The factors a and τ_3 are included in $v_{\rm ext}$ and $\sigma_{\rm MF}$ for convenience. After the ξ_p integration, Eq. (16) reduces to

$$[i\varepsilon\tau_3 - v_{\rm ext} - \sigma_{\rm MF}, \mathfrak{g}] = 0, \tag{18}$$

which is the equation to determine the quasiclassical propagator $\mathfrak{g}$. Notice that Eq. (18) holds for homogeneous systems. The mean-field self-energies $\sigma_{\rm MF}$ are composed of the Fermi-liquid corrections (diagonal parts) and the pair potentials (off-diagonal parts) as

$$\sigma_{\rm MF} = \begin{pmatrix} \Sigma_0 + \boldsymbol{\Sigma}\cdot\boldsymbol{\sigma} & \Delta \\ \bar{\Delta} & \bar{\Sigma}_0 + \bar{\boldsymbol{\Sigma}}\cdot\boldsymbol{\sigma}^{\rm tr} \end{pmatrix}. \tag{19}$$

The spin-triplet pair potentials are parametrized by

$$\Delta(\boldsymbol{p}_{\rm F}) = i\sigma_\mu\sigma_2 d_\mu(\boldsymbol{p}_{\rm F}) \tag{20}$$

and

$$\bar{\Delta}(\boldsymbol{p}_{\rm F}) = i\sigma_2\sigma_\mu d^*_\mu(\boldsymbol{p}_{\rm F}) \tag{21}$$

in terms of the three-dimensional vector $d_\mu(\boldsymbol{p}_{\rm F})$ ($\mu = 1, 2, 3$), which is called the $\boldsymbol{d}$ vector for the spin-triplet superfluidity. In the above equation, the sum is taken over μ. The explicit form of the $\boldsymbol{d}$ vector will be expressed by the Green's function in Eq. (37) in the next section. The solution of Eq. (18) is not uniquely determined *per se*, because $a + bg$ satisfies the same equation as g (a and b are arbitrary constants). To determine uniquely a solution for $\mathfrak{g}$, Eq. (18) must be supplemented by the normalization condition on the quasiclassical propagator $\mathfrak{g}^2 = -\pi^2\mathbb{I}$, with the unit matrix $\mathbb{I}$ in the NG space.

C. Mean-field self-energies and self-consistent equations

The interaction between two neutrons is modified by the polarization effects. In the vicinity of the Fermi surface, a perturbation that couples to the quasiparticle states generates a polarization of the fermionic vacuum. Such polarization leads to a correction to the self-energy with respect to the energy of a fermionic quasiparticle. The leading-order correction is given by mean-field interaction energy associated with a particle-hole excitation. As we mentioned above, the two-body interaction between fermionic quasiparticles is represented by a four-point renormalized vertex (Fig. 2)

$$\Gamma^{\rm ph}_{ab;cd}(p, p') = \Gamma^{\rm s}(p, p')\delta_{ac}\delta_{bd} + \Gamma^{\rm a}(p, p')\boldsymbol{\sigma}_{ac}\cdot\boldsymbol{\sigma}_{bd}, \tag{22}$$

which is composed of the amplitudes for spin-independent scattering ($\Gamma^{(\rm s)}$) and spin-dependent exchange scattering ($\Gamma^{(\rm a)}$), where $p \equiv (\boldsymbol{p}, \varepsilon)$. It sums the bare two-body interactions to all orders involving all possible intermediate states of high-energy fermions. We use the notation $(\boldsymbol{p}, -\boldsymbol{p})$ and $(\boldsymbol{p}', -\boldsymbol{p}')$ to stand for the incoming and outgoing momenta, respectively, for fermions 1 and 2. As the quasiclassical approximation takes account of quasiparticles confined to a low-energy shell near the Fermi surface, the vertex function can be evaluated with $\boldsymbol{p} = \boldsymbol{p}_{\rm F}$ and $\varepsilon \to 0$. The resulting vertex function reduces to

$$A^{(\rm s,a)}(\boldsymbol{p}_{\rm F}, \boldsymbol{p}'_{\rm F}) = 2N_{\rm F}\Gamma^{(\rm s,a)}(\boldsymbol{p} \approx \boldsymbol{p}_{\rm F}, \varepsilon = 0; \boldsymbol{p}' \approx \boldsymbol{p}'_{\rm F}, \varepsilon' = 0). \tag{23}$$

Then the scalar (Σ_0) and vector ($\boldsymbol{\Sigma}$) components in the diagonal parts in the mean-field self-energy $\sigma_{\rm MF}$ [Eq. (19)] are determined as

$$\Sigma_0(\boldsymbol{p}_{\rm F}) = T\sum_n \langle A^{(\rm s)}(\boldsymbol{p}_{\rm F}, \boldsymbol{p}'_{\rm F}) g_0(\boldsymbol{p}'_{\rm F}, \varepsilon_n)\rangle', \tag{24}$$

$$\boldsymbol{\Sigma}(\boldsymbol{p}_{\rm F}) = T\sum_n \langle A^{(\rm a)}(\boldsymbol{p}_{\rm F}, \boldsymbol{p}'_{\rm F}) \boldsymbol{g}(\boldsymbol{p}'_{\rm F}, \varepsilon_n)\rangle', \tag{25}$$

respectively, where $\sum_n$ denotes the Matsubara sum with the cutoff energy $\varepsilon_{\rm c}$ and

$$\langle\cdots\rangle' = \frac{1}{4\pi}\int d\theta'_{\boldsymbol{p}}\sin\theta'_{\boldsymbol{p}}\int d\phi'_{\boldsymbol{p}}\cdots \tag{26}$$

is the average over the Fermi surface with $\boldsymbol{p}' \approx |\boldsymbol{p}'_{\rm F}|(\cos\phi'_{\boldsymbol{p}}\sin\theta'_{\boldsymbol{p}}, \sin\phi'_{\boldsymbol{p}}\sin\theta'_{\boldsymbol{p}}, \cos\theta'_{\boldsymbol{p}})$ with the polar angles $\theta'_{\boldsymbol{p}}$ and $\phi'_{\boldsymbol{p}}$ for $\boldsymbol{p}'$.

Let $f(\boldsymbol{p}_1, \boldsymbol{p}_2)$ be the particle-hole interaction between two nucleons which is generalized in spin ($\boldsymbol{\sigma}$) and isospin ($\boldsymbol{\tau}$) spaces as

$$f(\boldsymbol{p}_1, \boldsymbol{p}_2) = N_{\rm F}\{F(\boldsymbol{p}_1, \boldsymbol{p}_2) + F'(\boldsymbol{p}_1, \boldsymbol{p}_2)\boldsymbol{\tau}_1\cdot\boldsymbol{\tau}_2 + G(\boldsymbol{p}_1, \boldsymbol{p}_2)\boldsymbol{\sigma}_1\cdot\boldsymbol{\sigma}_2 + G'(\boldsymbol{p}_1, \boldsymbol{p}_2)[\boldsymbol{\sigma}_1\cdot\boldsymbol{\sigma}_2][\boldsymbol{\tau}_1\cdot\boldsymbol{\tau}_2]\}, \tag{27}$$

where $\boldsymbol{p}_1$ ($\boldsymbol{p}_2$) is the three-dimensional momentum for the incoming (outgoing) particle and $\boldsymbol{\sigma}_1$ ($\boldsymbol{\sigma}_2$) and $\boldsymbol{\tau}_1$ ($\boldsymbol{\tau}_2$) stand for SU(2) spin and isospin interactions for the particle 1 (2). The first two terms with $F(\boldsymbol{p}_1, \boldsymbol{p}_2)$ and $F'(\boldsymbol{p}_1, \boldsymbol{p}_2)$ represent symmetric (spin-independent) quasiparticle scattering processes, while the latter two terms with $G(\boldsymbol{p}_1, \boldsymbol{p}_2)$ and $G'(\boldsymbol{p}_1, \boldsymbol{p}_2)$ represent the antisymmetric (spin-dependent) quasiparticle scattering processes. The single-particle momenta are taken at the Fermi surface $|\boldsymbol{p}_i| \approx |\boldsymbol{p}_{\rm F}|$ for $i = 1, 2$. We introduce the factor $N_{\rm F} = mp_{\rm F}/2\pi^2$ for the density of state of the fermion on the Fermi surface, so the parameters F, F', G, and G' are dimensionless quantities. Near the Fermi surface, F, F', G, and G' ($=\mathcal{G}$) are approximately regarded as functions only of the angle between $\boldsymbol{p}_1$ and $\boldsymbol{p}_2$, and thus they can be expanded in terms of the Legendre polynomials $P_\ell(x)$ ($\ell = 0, 1, 2, \ldots$),

$$\mathcal{G}(\boldsymbol{p}_{\rm F}\cdot\boldsymbol{p}'_{\rm F}) = \sum_\ell \mathcal{G}_\ell P_\ell(\boldsymbol{p}_{\rm F}\cdot\boldsymbol{p}'_{\rm F}), \tag{28}$$

for the function $\mathcal{G}(\boldsymbol{p}_{\rm F}\cdot\boldsymbol{p}'_{\rm F})$ depending on $\boldsymbol{p}_{\rm F}\cdot\boldsymbol{p}'_{\rm F}$. Here $\mathcal{G}_\ell$ is the coefficient in the channel ℓ. For neutron matter, one has $\boldsymbol{\tau}_1\cdot\boldsymbol{\tau}_2 = 1$ and the interaction potentials can be reduced to a more compact form by defining $F^{(\rm n)} = F + F'$ and $G^{(\rm n)} = G + G'$. The superscript (n) stands for the neutron matter. The self-energies describe the Fermi liquid corrections due to symmetric ($A^{(\rm s)}$) and antisymmetric ($A^{(\rm a)}$) quasiparticle scattering processes. The symmetric and antisymmetric quasiparticle scattering amplitudes are parametrized with the Landau Fermi-liquid parameters $F^{(\rm n)}_\ell$ and $G^{(\rm n)}_\ell$ as

$$A^{(\rm s)}(\boldsymbol{p}_{\rm F}, \boldsymbol{p}'_{\rm F}) = \sum_\ell \frac{F^{(\rm n)}_\ell}{1 + F^{(\rm n)}_\ell/(2\ell+1)} P_\ell(\boldsymbol{p}_{\rm F}\cdot\boldsymbol{p}'_{\rm F}) \tag{29}$$

for the spin-symmetric case and

$$A^{(\rm a)}(\boldsymbol{p}_{\rm F}, \boldsymbol{p}'_{\rm F}) = \sum_\ell \frac{G^{(\rm n)}_\ell}{1 + G^{(\rm n)}_\ell/(2\ell+1)} P_\ell(\boldsymbol{p}_{\rm F}\cdot\boldsymbol{p}'_{\rm F}) \tag{30}$$

for the spin-asymmetric case. We notice that, among several coefficients, $F^{(\rm n)}_{\ell=1}$ and $G^{(\rm n)}_{\ell=0}$ give the Fermi liquid corrections to the mass and spin susceptibility of a free neutron.

By taking into account the high-energy vertex corrections, the Zeeman energy in Eq. (5), $-\frac{1}{2}\gamma_{\rm n}\boldsymbol{\sigma}\cdot\boldsymbol{B}$, in the NG space is recast into

$$v_{\rm ext} = -\frac{1}{1 + G^{(\rm n)}_0}\begin{pmatrix} \frac{1}{2}\gamma_{\rm n}\boldsymbol{\sigma}\cdot\boldsymbol{B} & \boldsymbol{0} \\ \boldsymbol{0} & \frac{1}{2}\gamma_{\rm n}\boldsymbol{\sigma}^{\rm tr}\cdot\boldsymbol{B}\end{pmatrix}, \tag{31}$$

with the factor $1/(1 + G^{(\rm n)}_0)$. Here we introduce the magnetization density

$$\boldsymbol{M} = \boldsymbol{M}_{\rm N} + \frac{\gamma_{\rm n}N_{\rm F}}{1 + G^{(\rm n)}_0} T\sum_n \langle \boldsymbol{g}(\boldsymbol{p}_{\rm F}, \varepsilon_n)\rangle, \tag{32}$$

as a sum of the magnetization in the normal state and the correction by the superfluid state. The first term is explicitly given by $\boldsymbol{M}_{\rm N} = \chi_{\rm N}\boldsymbol{B}$, where $\chi_{\rm N} = \frac{1}{2}\gamma_{\rm n}^2 N_{\rm F}/(1+G_0^{(\rm n)})$ is the spin susceptibility renormalized by the Fermi-liquid correction ($G_0^{(\rm n)}$) in the normal state. The nonvanishing magnetization density $\boldsymbol{M}$ is fed back to the effective magnetic field $\boldsymbol{B}_{\rm eff}$ through the Fermi-liquid correction ($G_0^{(\rm n)}$),

$$v_{\rm ext} + \begin{pmatrix} \boldsymbol{\Sigma}\cdot\boldsymbol{\sigma} & \boldsymbol{0} \\ \boldsymbol{0} & \bar{\boldsymbol{\Sigma}}\cdot\boldsymbol{\sigma}^{\rm tr} \end{pmatrix} \equiv -\frac{1}{1+G_0^{(\rm n)}} \begin{pmatrix} \frac{1}{2}\gamma_{\rm n}\boldsymbol{\sigma}\cdot\boldsymbol{B}_{\rm eff} & \boldsymbol{0} \\ \boldsymbol{0} & \frac{1}{2}\gamma_{\rm n}\boldsymbol{\sigma}^{\rm tr}\cdot\boldsymbol{B}_{\rm eff} \end{pmatrix}, \quad (33)$$

with respect to Eqs. (31) and (32). Thus, the effective magnetic field including the corrections of the spin-polarization density is given by

$$\boldsymbol{B}_{\rm eff} = \left\{1 + G_0^{(\rm n)}\left(1 - \frac{M}{M_{\rm N}}\right)\right\}\boldsymbol{B}. \quad (34)$$

This gives rise to a nonlinear effect of the Zeeman magnetic field.

In the same manner, the polarization effects exist for the four-fermion vertex which is denoted by $\Gamma^{\rm pp}_{ab;cd}(\boldsymbol{p},\varepsilon;\boldsymbol{p}',\varepsilon')$ with the three-dimensional momentum $\boldsymbol{p}$ ($\boldsymbol{p}'$), the energy ε (ε'), and spin indices $a, c = \uparrow,\downarrow$ ($b, d = \uparrow,\downarrow$) for the incoming (outgoing) particles. This vertex is irreducible in the particle-particle channel that sums bare two-body interactions to all orders involving all possible intermediate states of high-energy fermions (Fig. 2). As fermion pairs with binding energy $|\Delta| \ll \varepsilon_{\rm c}$ are confined to a low-energy band near the Fermi surface $|\varepsilon| \leqslant \varepsilon_{\rm c} \ll \varepsilon_{\rm F}$, the particle-particle vertex varies slowly on $\boldsymbol{p}$ in the neighborhood of the Fermi surface. Thus, the vertex reduces to functions only of the relative momenta,

$$V_{ab;cd}(\boldsymbol{p}_{\rm F},\boldsymbol{p}'_{\rm F}) \equiv 2N_{\rm F}\Gamma^{\rm pp}_{ab;cd}(\boldsymbol{p}\approx\boldsymbol{p}_{\rm F},\varepsilon\to 0;\boldsymbol{p}'\approx\boldsymbol{p}'_{\rm F},\varepsilon'\to 0), \quad (35)$$

with the Fermi momenta $\boldsymbol{p}_{\rm F}$ and $\boldsymbol{p}'_{\rm F}$. The particle-particle vertex function is decomposed into the spin-singlet (even parity e) and spin-triplet (odd parity o) functions for the particle-particle channels

$$V_{ab;cd} = (i\sigma_y)_{ab}V^{(\rm e)}(i\sigma_y)_{cd} + (i\sigma_\mu\sigma_y)_{ab}V^{(\rm o)}_{\mu\nu}(i\sigma_y\sigma_\nu)_{cd}. \quad (36)$$

Using the effective interaction potential, one obtains the gap equation

$$d_\mu(\boldsymbol{p}_{\rm F}) = -T\sum_n \langle V^{(\rm o)}_{\mu\nu}(\boldsymbol{p}_{\rm F},\boldsymbol{p}'_{\rm F}) f_\nu(\boldsymbol{p}'_{\rm F},\varepsilon_n)\rangle', \quad (37)$$

with $\mu = 1, 2, 3$, which determines the equilibrium $\boldsymbol{d}$ vector $\boldsymbol{d} = (d_1, d_2, d_3)$. Here we have taken only the negative part of the ${}^3P_2$ channel (odd parity) as the effective pairing interaction for dense neutrons and have discarded the even-parity channel, i.e., $V^{(\rm e)} = 0$. The interaction in the ${}^3P_2$ channel is supposed to be the short-range one so that the momentum dependence can be safely neglected.

For the representation of the interaction potential, let us introduce the spherical tensors $\{t^{(m)}_{\mu i}\}_{m=-J,\ldots,+J}$, with $\mu, i = 1, 2, 3$, that form bases for representations of the rotational symmetry SO(3). Here $m = -J, \ldots, +J$ are the eigenvalues of J_z. For the ${}^3P_2$ channel, i.e., $J = 2$, the interaction potential can be expressed as the separable form of the symmetric and traceless tensors as

$$V^{(\rm o)}_{\mu\nu}(\boldsymbol{p}_{\rm F},\boldsymbol{p}'_{\rm F}) = -v\sum_{m=-J}^{J}\sum_{i,j=1}^{3}\left[t^{(m)}_{\mu i}p_{{\rm F},i}\right]\left[t^{(m)}_{\nu j}p'_{{\rm F},j}\right]^*, \quad (38)$$

where $v > 0$ is the coupling constant of the zero-range attractive ${}^3P_2$ interaction. Here $p_{{\rm F},i}$ ($p'_{{\rm F},j}$) is the ith (jth) component of the three-dimensional momentum $\boldsymbol{p}_{\rm F}$ ($\boldsymbol{p}'_{\rm F}$) for the incoming (outgoing) states of the scattering neutron. It is important that the momentum dependence appears because the P-wave interaction potential is adopted. Equation (38) is recast into

$$V^{(\rm o)}_{ab;cd}(\boldsymbol{p}_{\rm F},\boldsymbol{p}'_{\rm F}) = -v\sum_{\mu,\nu=1}^{3} T_{\mu\nu,ab}(\boldsymbol{p}_{\rm F})T^*_{\mu\nu,dc}(\boldsymbol{p}'_{\rm F}), \quad (39)$$

with the traceless and symmetric tensor

$$T_{\mu\nu,ab}(\boldsymbol{p}_{\rm F}) = \left[i\left(\frac{1}{2\sqrt{2}}(\sigma_\mu p_{{\rm F},\nu} + \sigma_\nu p_{{\rm F},\mu}) - \frac{1}{3\sqrt{2}}\delta_{\mu\nu}\boldsymbol{\sigma}\cdot\boldsymbol{p}_{\rm F}\right)\sigma_y\right]_{ab}, \quad (40)$$

which obeys $T_{\mu\nu}(\boldsymbol{p}_{\rm F}) = T_{\nu\mu}(\boldsymbol{p}_{\rm F})$ and $\mathrm{tr}[T(\boldsymbol{p}_{\rm F})] \equiv \sum_\mu T_{\mu\mu}(\boldsymbol{p}_{\rm F}) = 0$ [28].

The order parameter of spin-triplet superfluids $\boldsymbol{d}(\boldsymbol{p}_{\rm F})$ is parametrized as

$$d_\mu(\boldsymbol{p}_{\rm F}) = \sum_{i=1}^{3} A_{\mu i}\hat{p}_i, \quad (41)$$

with the rank-2 tensor $A_{\mu i}$, where the index μ (i) denotes the spin (orbital) degrees of freedom of the Cooper pair and we have introduced $\hat{\boldsymbol{p}} = (\hat{p}_1, \hat{p}_2, \hat{p}_3)$ with $\hat{\boldsymbol{p}} \equiv \hat{\boldsymbol{p}}_{\rm F}/p_{\rm F}$. In general, a rank-2 tensor can be expanded as a sum of the terms of the total angular momenta $J = 0$, 1, and 2 as

$$A_{\mu i} = \mathcal{A}^{(0)}\delta_{\mu i} + \mathcal{A}^{(1)}_{\mu i} + \mathcal{A}^{(2)}_{\mu i}, \quad (42)$$

where the scalar function $\mathcal{A}^{(0)} \equiv \mathrm{tr}(A)/3$, the antisymmetric matrix $\mathcal{A}^{(1)}_{\mu i} \equiv (A_{\mu i} - A_{i\mu})/2$, and the symmetric traceless matrix $\mathcal{A}^{(2)}_{\mu i} \equiv (A_{\mu i} + A_{i\mu})/2 - \frac{1}{3}\delta_{\mu i}\mathrm{tr}(A)$ are the eigenstates of $J = 0$, 1, and 2, respectively. Thus, the number of independent components in $A_{\mu i}$ is then given as $\mathbf{3}\otimes\mathbf{3} = \mathbf{1}\oplus\mathbf{3}\oplus\mathbf{5}$, where the numbers on the right-hand side represent the multiplicities of eigenstates of the total angular momenta $J = 0$, 1, and 2, respectively. In the following, we consider the neutron ${}^3P_2$ superfluidity. Thus, we neglect the $J = 0$ and 1 components ($\mathcal{A}^{(0)} = \mathcal{A}^{(1)}_{\mu i} = 0$) and express the tensor of the ${}^3P_2$ order parameter by $A_{\mu i} = \mathcal{A}^{(2)}_{\mu i}$. Then $A_{\mu i}$ is determined by solving the gap equation

$$A_{\mu i} = \tfrac{1}{2}[\mathcal{F}_{\mu i} + \mathcal{F}_{i\mu}] - \tfrac{1}{3}\delta_{\mu i}\mathrm{tr}[\mathcal{F}], \quad (43)$$

with

$$\mathcal{F}_{\mu i} \equiv vT\sum_n \langle f_\mu(\boldsymbol{p}'_{\rm F},\varepsilon_n)\hat{p}'_i\rangle', \quad (44)$$

where the average calculation for the momentum has been adopted from Eq. (26).

In calculating Eqs. (43) and (44), we utilize the fact that the cutoff energy ε_c and the coupling constant v are related to a measurable quantity, i.e., the bulk transition temperature T_c, through linearized gap equation

$$\frac{1}{v} = \frac{5}{9}\pi T \sum_{|\varepsilon_n|<\varepsilon_c} \frac{1}{|\varepsilon_n|} \approx \frac{5}{9} \ln \frac{1.13\varepsilon_c}{T}. \tag{45}$$

Eliminating ε_c and v from the above gap equation, Eq. (44) reduces to

$$\left(\ln \frac{T}{T_c}\right)\mathcal{F}_{\mu i} = 3T \sum_n \langle f_\mu(\boldsymbol{p}'_F, \varepsilon_n)\hat{p}'_i\rangle' - \sum_n \frac{\pi T}{|\varepsilon_n|}. \tag{46}$$

This is free from the ultraviolet divergence. Thus, the regularization of the gap equation leads to rapidly convergent series defined in terms of T_c.

D. Thermodynamic potential

The thermodynamic potential in Eq. (6), which is the Φ functional, generates the diagonal components and the off-diagonal components in the self-energy (8). To derive the thermodynamic potential within the quasiclassical approximation, we subtract the normal-state contributions from the Luttinger-Ward functional as $\Delta\Omega \equiv \Omega[G, \Sigma] - \Omega[G_N, \Sigma_N]$, where G_N and Σ_N are the Green's function and self-energy in the normal state, respectively. In this approximation, the Luttinger-Ward thermodynamic potential is then given by [99,100]

$$\Delta\Omega[\mathfrak{g}] = \frac{1}{2}\int_0^1 d\lambda\, \mathrm{Sp}'\{\sigma_{\rm MF}(\mathfrak{g}_\lambda - \mathfrak{g})\} + \Delta\Phi[\mathfrak{g}], \tag{47}$$

where $\Delta\Phi[\mathfrak{g}]$ is the Φ functional confined to the low-energy region of the phase space. In the diagrammatic representation, $\Delta\Phi$ is formally constructed by low-energy propagators ($G^{\rm low}$), and the higher-energy propagator ($G^{\rm high}$) is renormalized into vertices as in Fig. 2. In Eq. (47) we set

$$\mathrm{Sp}'\{\cdots\} \equiv N_F T \sum_n \langle\cdots\rangle. \tag{48}$$

The quasiclassical auxiliary function g_λ is given by replacing $\sigma_{\rm MF} \to \lambda\sigma_{\rm MF}$ in Eq. (18). Here we determine the quasiclassical Φ functional so as to consistently generate the self-energy through the functional derivative $\sigma_{\rm MF} = 2\delta\Delta\Phi[\mathfrak{g}]/\delta\mathfrak{g}^{\rm tr}$. It is found that the Φ functional is constructed as

$$\Delta\Phi[\mathfrak{g}] = \tfrac{1}{4}\mathrm{Sp}'\{\sigma_{\rm MF}\mathfrak{g}\}, \tag{49}$$

which generates the self-consistent equations (24), (25), and (37).

E. Critical exponents and universality class

The superfluid states subject to the total angular momentum $J = 2$ are classified into several phases: uniaxial/biaxial nematic phases, the ferromagnetic phase, and the cyclic phase [55,61,81]. The nematic phases preserve the time-reversal symmetry and occupy the region of the phase diagram under a uniform magnetic field, while the latter two are nonunitary states with spontaneously broken time-reversal symmetry. The ground state at the weak-coupling limit is the uniaxial/biaxial nematic phase in which the rank-2 tensor $A_{\mu i}$ is represented by

$$A_{\mu i}(T, B) = \Delta(T, B)\begin{pmatrix} 1 & 0 & 0 \\ 0 & r(T, B) & 0 \\ 0 & 0 & -1 - r(T, B) \end{pmatrix}_{\mu i}, \tag{50}$$

where $\Delta = \Delta(T, B) \geqslant 0$ is the amplitude and $r = r(T, B) \in [-1, -1/2]$ is the internal parameter that characterizes the biaxiality of the nematic state. The state with $r = -1/2$ is called the uniaxial nematic phase where $A_{\mu i}$ is invariant under D_∞ including SO(2). The state with $r = -1$ is called the D_4-biaxial nematic phase where $A_{\mu i}$ is invariant under dihedral-four symmetry with C_4 and C_2 axes. The intermediate r is called the D_2-biaxial nematic phase where $A_{\mu i}$ is invariant under dihedral-two symmetry with three C_2 axes.[9] The order parameters $\Delta(T, B)$ and $r(T, B)$ are determined by self-consistently solving the quasiclassical equation (18), the spin polarization in Eq. (25), and the gap equation (43). Notice that we consider a spatially uniform magnetic field along the z axis, without loss of generality: $\boldsymbol{B} = (0, 0, B)$.

Let us consider the phase diagram on the T-B plane. Figures 1(a) and 1(b) show the phase diagram of $^3P_2$ superfluids under a magnetic field for the Landau parameter $G_0^{(n)} = -0.7$ and -0.4, respectively. The UN phase ($r = -1/2$) is thermodynamically stable in zero fields, while the magnetic field drives the transition from the D_2-BN phase ($-1 < r < -1/2$) to the D_4-BN phase ($r = -1$). The behavior of r on the T-B plane is shown in detail in Fig. 3(a). In this figure, we find that r continuously reduces to -1 with increasing T in the lower-B region, and hence the D_2-BN state undergoes the second-order phase transition to the D_4-BN state. Under higher-B fields, however, the order parameter r shows the finite jump at a finite B, leading to the first-order phase transition from the D_2-BN phase to the D_4-BN phase, as indicated by open circles in the figure. The first- and second-order phase boundaries meet at the critical end point at $(T_{\rm CEP}/T_c, \gamma_n B_{\rm CEP}/\pi T_c) \approx (0.489\,50, 0.079\,063)$ for $G_0^{(n)} = -0.7$ and at $(0.285\,68, 0.184\,375)$ for $G_0^{(n)} = -0.4$.

We remark that the first-order transition and the CEP are attributed to the screening effect of the external magnetic field due to the spin-polarized molecular field. The magnetic Zeeman field gives rise to the Pauli paramagnetic depairing of the uniaxial nematic state that suppresses the component of the $\boldsymbol{d}$ vector along the $\boldsymbol{B}$ field, i.e., $|A_{zz}|/\Delta = 1 + r < 1/2$ in Eq. (50) for $B \neq 0$. The suppression of the magnetization in the D_2-BN state, $|\boldsymbol{M}| < M_N$, is fed back to the effective magnetic field in Eq. (34), giving rise to the screening of the external magnetic field, $|\boldsymbol{B}_{\rm eff}| < B$, for $G_0^{(n)} < 0$. In contrast, the D_4-BN state always satisfies the configuration $\boldsymbol{d} \perp \boldsymbol{H}$, which is most favored under $\boldsymbol{B}$ and free from the paramagnetic depairing, i.e., $\boldsymbol{M} = \boldsymbol{M}_N$ and $\boldsymbol{B}_{\rm eff} = \boldsymbol{B}$. As $G_0^{(n)}$ approaches the Pomeranchuk instability at $G_0^{(n)} = -1$, therefore, the D_4-BN phase can be stabilized in lower fields and the position of the CEP shifts to the region of lower fields and higher temperatures. We note that the position of the CEP reads $(T_{\rm CEP}/T_c, \gamma_n B_{\rm CEP}/\pi T_c) \approx (0.489\,50, 0.079\,063)$,

[9] See, e.g., Appendix B in Refs. [80,91] for more information on the definitions of the UN, D_2-BN, and D_4-BN phases.

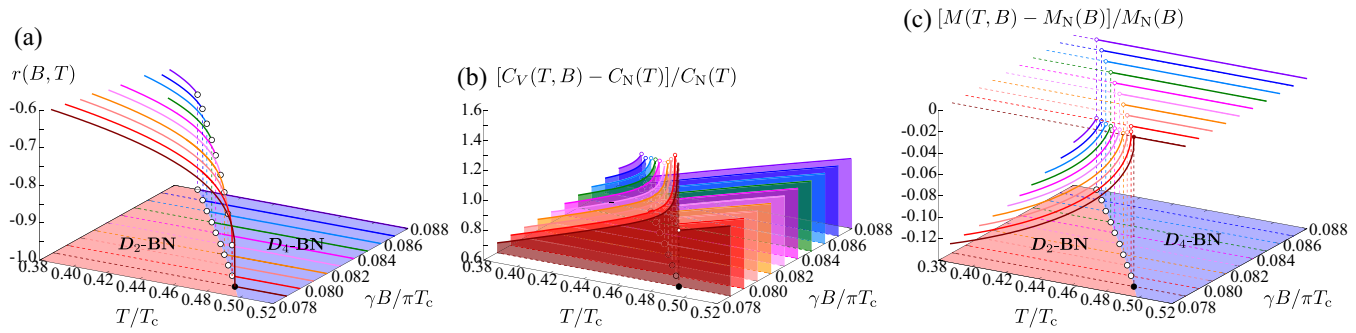

FIG. 3. (a) Temperature dependence of the order parameter $r(B, T)$. (b) Heat capacity $C_S(T, B)$. (c) Magnetization $M(T, B) - M_N(B) \equiv -\partial\delta\Omega/\partial B$ around the CEP. The open (closed) circles correspond to the first-order (second-order) phase transition between D_2-BN and D_4-BN states. Here we set $G_0^{(n)} = -0.7$.

(0.285 68, 0.184 375), (0.2225, 0.248 75), and (0.15,0.3111) for $G_0^{(n)} = -0.7$, -0.4, -0.2, and 0, respectively. The CEP shifts toward low temperatures with $G_0^{(n)} \to -\eta$ with a small positive number η $(0 < \eta \ll 1)$ and vanishes at a positive value of $G_0^{(n)}$.

The consequence of the CEP is captured by thermodynamic quantities. In Fig. 3(b) we plot the heat capacity in the superfluid state per volume $C(T, B)$, which is obtained from the Luttinger-Ward thermodynamic potential $\Delta\Omega[\mathfrak{g}]$ as

$$C_V(T, B) \equiv C_N(T) - T\frac{\partial^2\Delta\Omega}{\partial T^2}, \tag{51}$$

where the heat capacity of the normal gas of neutrons is given by $C_N(T) = (2\pi^2/3)N_F k_B^2 T$. The heat capacity contains critical information on the thermal evolution of neutron stars [12]. The heat capacity shows the jump at the lower T. Another quantity which captures the consequence of the CEP is the magnetization M. This is defined as the first derivative of $\Delta\Omega$,

$$M(T, B) = M_N(B) - \frac{\partial\Delta\Omega}{\partial B}, \tag{52}$$

which coincides with Eq. (32). It can be seen from Fig. 3(c) that the T dependence on M has a jump in the higher-B region, indicating the first-order phase transition from the D_2-BN phase to the D_4-BN phase. The jump in M decreases as the magnetic field approaches the CEP. The discontinuity of M implies the divergence of the spin susceptibility,

$$\chi(T, B) = \frac{\partial M}{\partial B} = \chi_N - \frac{\partial^2\Delta\Omega}{\partial B^2}. \tag{53}$$

To extract the critical behaviors of the $^3P_2$ superfluids, we compute the critical exponents around the CEP at (T_{CEP}, B_{CEP}). We note that the contributions of the normal gas of neutrons to Eqs. (51) and (52), $C_N(T)$ and $M_N(B)$, are negligible in the vicinity of the CEP, and the critical behaviors of the heat capacity C_V, the magnetization M, and the spin susceptibility χ are governed by the superfluid contributions

$$C_V(T, B) \approx -T\frac{\partial^2\Delta\Omega}{\partial T^2}, \tag{54}$$

$$M(T, B) \approx -\frac{\partial\Delta\Omega}{\partial B}, \tag{55}$$

$$\chi(T, B) \approx -\frac{\partial^2\Delta\Omega}{\partial B^2}. \tag{56}$$

Then we consider the set of the critical exponents $(\alpha, \beta, \gamma, \delta)$ from the scaling behavior, which are parametrized by

$$C_V(T, B_{CEP}) - C_V(T_{CEP}, B_{CEP}) \propto |T - T_{CEP}|^{-\alpha}, \tag{57}$$

$$M(T, B_{CEP}) - M(T_{CEP}, B_{CEP}) \propto |T - T_{CEP}|^{\beta}, \tag{58}$$

$$M(T_{CEP}, B) - M(T_{CEP}, B_{CEP}) \propto |B - B_{CEP}|^{1/\delta}, \tag{59}$$

$$\chi(T, B_{CEP}) - \chi(T_{CEP}, B_{CEP}) \propto |T - T_{CEP}|^{-\gamma} \tag{60}$$

for $T < T_{CEP}$ and $B < B_{CEP}$. Under the scaling hypothesis, the set of critical exponents $(\alpha, \beta, \gamma, \delta)$ satisfies the three equalities in Eqs. (1)–(3), i.e., the Rushbrooke, Griffiths, and Widom equalities, which should hold at the CEP for any systems irrespective of the different interactions and dimensions. These three relations relate the critical exponents of magnetic systems, which have the end point of a first-order phase transition at nonzero temperatures.

Figure 4 shows the scaling behavior of the specific heat $C_V(T, B)$, the magnetization $M(T, B)$, and the spin susceptibility $\chi(T, B)$ around the CEP (T_{CEP}, B_{CEP}), which are directly computed with self-consistent solutions of the superfluid Fermi liquid theory. From these data, we read the values of the critical exponents as

$$\alpha = 0.68, \quad \beta = 0.41, \quad \gamma = 0.57, \quad \delta = 2.3 \tag{61}$$

for $G_0^{(n)} = -0.7$. We find that the values of Eq. (61) satisfy the three equalities (1)–(3) within the error range of 10% at most,

$$\alpha + 2\beta + \gamma = 2.07, \tag{62}$$

$$\alpha + \beta(1 + \delta) = 2.03, \tag{63}$$

$$-\frac{\gamma}{\beta} + \delta = 0.91, \tag{64}$$

indicating that the superfluid Fermi liquid theory properly captures the critical behavior of the CEP in neutron $^3P_2$ superfluids. For $G_0^{(n)} = -0.4$, we read $(\alpha, \beta, \gamma, \delta) = (0.60, 0.45, 0.59, 2.3)$ from the data in Fig. 4, which satisfy the above equalities within the error range of 5% at most, such that $\alpha + 2\beta + \gamma = 2.09$, $\alpha + \beta(1 + \delta) = 2.09$, and $-\frac{\gamma}{\beta} + \delta = 0.99$. In Table I we summarize the values of

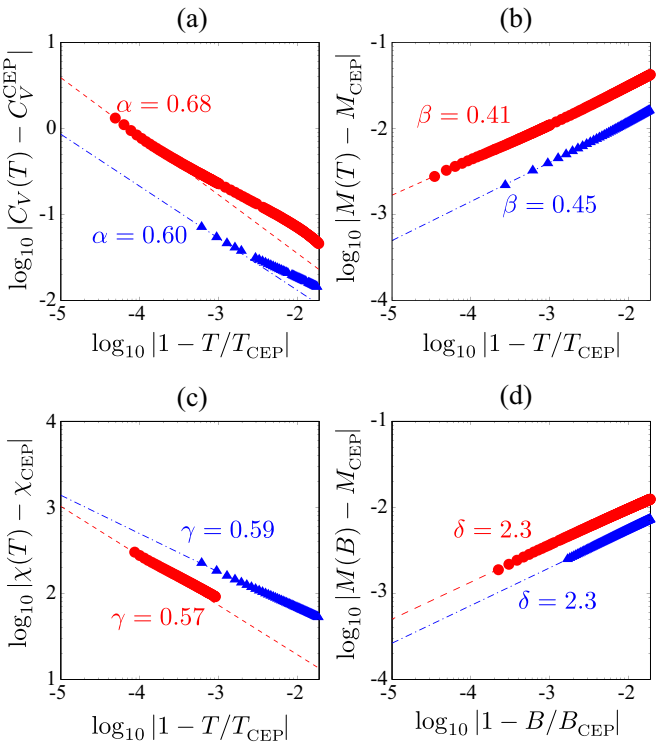

FIG. 4. Scaling behavior of $C_V(T, B_{\rm CEP})$, $M(T, B_{\rm CEP})$, $M(T_{\rm CEP}, B)$, and $\chi(T, B_{\rm CEP})$ around the CEP $(T_{\rm CEP}/T_c, \gamma_n B_{\rm CEP}/\pi T_c) \approx (0.489\,50, 0.079\,063)$ for $G_0^{(n)} = -0.7$ (circles) and $(0.285\,68, 0.184\,375)$ for $G_0^{(n)} = -0.4$ (triangles). Here we set $C_V(T) \equiv C_V(T, B_{\rm CEP})$, $M(T) \equiv M(T, B_{\rm CEP})$, $M(B) \equiv M(T_{\rm CEP}, B)$, $\chi(T) \equiv \chi(T, B_{\rm CEP})$, $C_V^{\rm CEP} \equiv C_V(T_{\rm CEP}, B_{\rm CEP})$, $M_{\rm CEP} \equiv M(T_{\rm CEP}, B_{\rm CEP})$, and $\chi_{\rm CEP} \equiv \chi(T_{\rm CEP}, B_{\rm CEP})$.

the critical exponents $(\alpha, \beta, \gamma, \delta)$ for the Landau parameters $G_0^{(n)} = -0.7$ and -0.4. It turns out that the resulting exponents are insensitive to the screening effect of the external magnetic field due to the spin-polarized molecular field.

We propose that the set of critical exponents $(\alpha, \beta, \gamma, \delta)$ in Eq. (61) belongs to a different type of university class. First of all, one may notice the large value of α ($\alpha \sim 0.6$). It is known that the value of α is usually much smaller than one in the phase transitions accompanied by a continuous symmetry breaking at least in known models thus far. However, the value of α can be larger in cases accompanied by discrete symmetry breaking, such as the Potts model in two dimensions [93,94]. In our case, the CEP appears in the phase transition with a discrete symmetry breaking, i.e., from D_2 to D_4. Thus, it may be natural to have the large value of α in the neutron $^3P_2$ superfluid. Phenomenologically, the large α indicates that the heat capacity is much enhanced at the CEP [cf. Eq. (57)], which may affect the cooling process in the evolution of neutron stars. Naively one may say that the large heat capacity will lead to a slow cooling in the evolution of neutron stars.

TABLE I. Critical exponents $(\alpha, \beta, \gamma, \delta)$ computed by the superfluid Fermi liquid theory with $G_0^{(n)} = -0.7$ and -0.4 in the BdG theory and the GL theory. The Fermi liquid correction with $G^{(n)} < 0$ leads to the screening effect of a magnetic field due to the spin-polarized molecular field. Note that the values of the critical exponents in the GL theory are independent of $G_0^{(n)}$.

Theory	$G_0^{(n)}$	α	β	γ	δ
BdG	-0.7	0.68	0.41	0.57	2.3
BdG	-0.4	0.60	0.45	0.59	2.3
GL		0.60	0.49	0.52	1.95

Another feature of the critical exponents in Eq. (61) is that the value of γ is smaller than one ($\gamma \sim 0.5$). In the literature, there is only a limited number of examples which indicate $\gamma < 1$. One example is the O(n) model with $n < 0$ [95]. The O(n) model induces the Ising model at $n = 1$ and the self-avoiding polymer/walk model at $n = 0$. If the value of γ is expressed in the asymptotic series up to the second-order terms in the vicinity of four dimensions, it is found that γ can be smaller than one if n is extrapolated to the negative region ($n < 0$). Another example for $\gamma < 1$ is the tricritical Ising model coupled to massless Dirac fermions [96]. In conclusion, the large α and the small γ are unique features of the critical exponents in the neutron $^3P_2$ superfluid, implying a different universality class.

III. GINZBURG-LANDAU THEORY FOR THE CRITICAL END POINT

A. Ginzburg-Landau free energy

Let us turn to a discussion based on the GL theory [27,28,55–60,80,89–91]. In the weak-coupling limit for the neutron-neutron interaction, we obtain the GL free-energy density

$$\Delta\Omega[A] = \Omega_8^{(0)}[A] + \Omega_2^{(\leqslant 4)}[A] + \Omega_4^{(\leqslant 2)}[A] + O(B^m A^n)_{m+n\geqslant 7}, \tag{65}$$

as an expansion series in terms of the condensate $A_{\mu i}$ and the magnetic field $\boldsymbol{B}$ [89,91]. We have adopted the quasiclassical approximation for the momentum integrals for the neutron loops. Notice that the free-energy part for the noninteracting neutron is not included, because it is irrelevant to the condensate. Each term in Eq. (65) is explained as follows: $\Omega_8^{(0)}[A]$ includes $A_{\mu i}$ up to the eighth order with no magnetic field, $\Omega_2^{(\leqslant 4)}[A]$ includes $A_{\mu i}$ up to the second order with the magnetic field up to $|\boldsymbol{B}|^4$, and $\Omega_4^{(\leqslant 2)}[A]$ includes $A_{\mu i}$ up to the fourth order with the magnetic field up to $|\boldsymbol{B}|^2$. Their explicit forms are

$$\Omega_8^{(0)}[A] = K^{(0)} \sum_{i,j,\mu=1,2,3} (\nabla_j A_{i\mu}^* \nabla_j A_{\mu i} + \nabla_i A_{i\mu}^* \nabla_j A_{\mu j} + \nabla_i A_{j\mu}^* \nabla_j A_{\mu i}) + \alpha^{(0)}({\rm tr}A^*A) + \beta^{(0)}[({\rm tr}A^*A)^2 - ({\rm tr}A^{*2}A^2)]$$
$$+ \gamma^{(0)}[-3({\rm tr}A^*A)({\rm tr}A^2)({\rm tr}A^{*2}) + 4({\rm tr}A^*A)^3 + 6({\rm tr}A^*A)({\rm tr}A^{*2}A^2) + 12({\rm tr}A^*A)({\rm tr}A^*AA^*A)$$
$$- 6({\rm tr}A^{*2})({\rm tr}A^*A^3) - 6({\rm tr}A^2)({\rm tr}A^{*3}A) - 12({\rm tr}A^{*3}A^3) + 12({\rm tr}A^{*2}A^2A^*A) + 8({\rm tr}A^*AA^*AA^*A)]$$

$$
\begin{aligned}
&+\delta^{(0)}[(\mathrm{tr}A^{*2})^2(\mathrm{tr}A^2)^2+2(\mathrm{tr}A^{*2})^2(\mathrm{tr}A^4)-8(\mathrm{tr}A^{*2})(\mathrm{tr}A^*AA^*A)(\mathrm{tr}A^2)-8(\mathrm{tr}A^{*2})(\mathrm{tr}A^*A)^2(\mathrm{tr}A^2)\\
&-32(\mathrm{tr}A^{*2})(\mathrm{tr}A^*A)(\mathrm{tr}A^*A^3)-32(\mathrm{tr}A^{*2})(\mathrm{tr}A^*AA^*A^3)-16(\mathrm{tr}A^{*2})(\mathrm{tr}A^*A^2A^*A^2)\\
&+2(\mathrm{tr}A^{*4})(\mathrm{tr}A^2)^2+4(\mathrm{tr}A^{*4})(\mathrm{tr}A^4)-32(\mathrm{tr}A^{*3}A)(\mathrm{tr}A^*A)(\mathrm{tr}A^2)-64(\mathrm{tr}A^{*3}A)(\mathrm{tr}A^*A^3)\\
&-32(\mathrm{tr}A^{*3}AA^*A)(\mathrm{tr}A^2)-64(\mathrm{tr}A^{*3}A^2A^*A^2)-64(\mathrm{tr}A^{*3}A^3)(\mathrm{tr}A^*A)-64(\mathrm{tr}A^{*2}AA^{*2}A^3)\\
&-64(\mathrm{tr}A^{*2}AA^*A^2)(\mathrm{tr}A^*A)+16(\mathrm{tr}A^{*2}A^2)^2+32(\mathrm{tr}A^{*2}A^2)(\mathrm{tr}A^*A)^2+32(\mathrm{tr}A^{*2}A^2)(\mathrm{tr}A^*AA^*A)\\
&+64(\mathrm{tr}A^{*2}A^2A^{*2}A^2)-16(\mathrm{tr}A^{*2}AA^{*2}A)(\mathrm{tr}A^2)+8(\mathrm{tr}A^*A)^4+48(\mathrm{tr}A^*A)^2(\mathrm{tr}A^*AA^*A)\\
&+192(\mathrm{tr}A^*A)(\mathrm{tr}A^*AA^{*2}A^2)+64(\mathrm{tr}A^*A)(\mathrm{tr}A^*AA^*AA^*A)-128(\mathrm{tr}A^*AA^{*3}A^3)\\
&+64(\mathrm{tr}A^*AA^{*2}AA^*A^2)+24(\mathrm{tr}A^*AA^*A)^2+128(\mathrm{tr}A^*AA^*AA^{*2}A^2)+48(\mathrm{tr}A^*AA^*AA^*AA^*A)],
\end{aligned}
\tag{66}
$$

$$
\Omega_2^{(\leqslant 4)}[A]=\beta^{(2)}\boldsymbol{B}^tA^*A\boldsymbol{B}+\beta^{(4)}|\boldsymbol{B}|^2\boldsymbol{B}^tA^*A\boldsymbol{B},
\tag{67}
$$

$$
\begin{aligned}
\Omega_4^{(\leqslant 2)}[A]=\gamma^{(2)}[&-2|\boldsymbol{B}|^2(\mathrm{tr}A^2)(\mathrm{tr}A^{*2})-4|\boldsymbol{B}|^2(\mathrm{tr}A^*A)^2+4|\boldsymbol{B}|^2(\mathrm{tr}A^*AA^*A)+8|\boldsymbol{B}|^2(\mathrm{tr}A^{*2}A^2)\\
&+\boldsymbol{B}^tA^2\boldsymbol{B}(\mathrm{tr}A^{*2})-8\boldsymbol{B}^tA^*A\boldsymbol{B}(\mathrm{tr}A^*A)+\boldsymbol{B}^tA^{*2}\boldsymbol{B}\big(\mathrm{tr}A^2\big)+2\boldsymbol{B}^tAA^{*2}A\boldsymbol{B}\\
&+2\boldsymbol{B}^tA^*A^2A^*\boldsymbol{B}-8\boldsymbol{B}^tA^*AA^*A\boldsymbol{B}-8\boldsymbol{B}^tA^{*2}A^2\boldsymbol{B}],
\end{aligned}
\tag{68}
$$

with the derivative ∇_i for the spatial directions $i=1,2,3$ and the GL coefficients defined by

$$
\begin{aligned}
&K^{(0)}=\frac{7\zeta(3)N_{\mathrm{F}}p_F^4}{240m^2(\pi T_{\mathrm{c}})^2},\quad \alpha^{(0)}=\frac{N_{\mathrm{F}}p_F^2}{3}\ln\frac{T}{T_{\mathrm{c}}},\\
&\beta^{(0)}=\frac{7\zeta(3)N_{\mathrm{F}}p_F^4}{60(\pi T_{\mathrm{c}})^2},\quad \beta^{(2)}=\frac{7\zeta(3)N_{\mathrm{F}}p_F^2\gamma_{\mathrm{n}}^2}{48(1+G_0^{(\mathrm{n})})^2(\pi T_{\mathrm{c}})^2},\\
&\beta^{(4)}=-\frac{31\zeta(5)N_{\mathrm{F}}p_F^2\gamma_{\mathrm{n}}^4}{768(1+G_0^{(\mathrm{n})})^4(\pi T_{\mathrm{c}})^4},\quad \gamma^{(0)}=-\frac{31\zeta(5)N_{\mathrm{F}}p_F^6}{13\,440(\pi T_{\mathrm{c}})^4},\\
&\gamma^{(2)}=\frac{31\zeta(5)N_{\mathrm{F}}p_F^4\gamma_{\mathrm{n}}^2}{3840(1+G_0^{(\mathrm{n})})^2(\pi T_{\mathrm{c}})^4},\quad \delta^{(0)}=\frac{127\zeta(7)N_{\mathrm{F}}p_F^8}{387\,072(\pi T_{\mathrm{c}})^6}.
\end{aligned}
\tag{69}
$$

Here $\zeta(n)$ is the zeta function. In the above expression, $\boldsymbol{\mu}_n$ has been replaced by $\boldsymbol{\mu}_n^*=(\gamma_{\mathrm{n}}/2)\boldsymbol{\sigma}/(1+G_0^{(\mathrm{n})})$, i.e., the magnetic momentum of a neutron modified by the Landau parameter $G_0^{(\mathrm{n})}$. We note that the Landau parameter stems from the Hartree-Fock approximation, which is not taken into account explicitly in the present procedure for the fermion-loop expansion. The choice of the value of $G_0^{(\mathrm{n})}$ does not affect the values of the critical exponents because the magnetic field is scaled uniformly. This is different from the analysis in the BdG equation in Sec. II, where the spin polarization leads to the nonlinear effect for the Zeeman magnetic field [cf. Eq. (34)].

We notice that the $\beta^{(4)}$ and $\gamma^{(2)}$ terms were derived beyond the leading-order term for the magnetic field [89] and the $\delta^{(0)}$ term was calculated to recover the global stability of the ground state which was absent at the sixth order [91]. We emphasize that, as discussed in detail in Ref. [91], the $\delta^{(0)}$ term (the eighth-order term) produces the first-order transition in the GL equation, which was absent in the analysis up to the sixth-order term, and hence it leads to the existence of the CEP in the GL equation. In the derivation of the GL equation, we have supposed that the temperature T is close to the critical temperature at zero magnetic field T_{c}, and hence the applicable region of the GL equation is limited to $|1-T/T_{\mathrm{c}}|\ll 1$. Note that the critical temperature is the unique energy scale in the GL theory in the above discussion.

B. Critical end point of $^3P_2$ superfluid phase diagrams

Let us consider the phase diagram drawn by the variational calculation for the GL free energy. For the magnetic field as $\boldsymbol{B}=(0,0,B)$, we consider the minimization of the GL free energy with respect to Δ and r in Eq. (50). We show the phase diagram on the plane spanned by the temperature (T/T_{c}) and the magnetic field $(\gamma_{\mathrm{n}}B/\pi T_{\mathrm{c}})$ in Fig. 1(d). The CEP is $(T_{\mathrm{CEP}}/T_{\mathrm{c}},\gamma_{\mathrm{n}}B_{\mathrm{CEP}}/\pi T_{\mathrm{c}})=(0.774\,597,0.004\,465)$. The phase boundary at $T<T_{\mathrm{CEP}}$ and $B<B_{\mathrm{CEP}}$ is the first-order transition, as indicated by the cyan lines in the figure. It should be noted that the existence of the CEP is due to the eighth-order term as it was discovered in previous work [91]. Thus, the GL theory shares common properties with the BdG theory about the existence of the CEP, though the positions of the CEPs are different.

We consider the thermodynamical quantities, i.e., the heat capacity, the magnetization, and the spin susceptibility, which have been introduced in Eqs. (54)–(56), and investigate their scaling behaviors at the CEP. Around the critical end point, we introduce the critical exponents α, β, γ, and δ for the heat capacity, the magnetization, and the spin susceptibility as defined in Eqs. (57)–(60). We plot $C_V(T,B)$, $M(T,B)$, and $\chi(T,B)$ in Fig. 5. From those plots we find that the values of the critical exponents read

$$
\alpha=0.60,\quad \beta=0.49,\quad \gamma=0.52,\quad \delta=1.95.
\tag{70}
$$

When we substitute the values from Eq. (70) into the left-hand sides of the identities (1)–(3) we obtain

$$
\alpha+2\beta+\gamma=2.10,
\tag{71}
$$

$$
\alpha+\beta(1+\delta)=2.04,
\tag{72}
$$

$$
-\frac{\gamma}{\beta}+\delta=1.11.
\tag{73}
$$

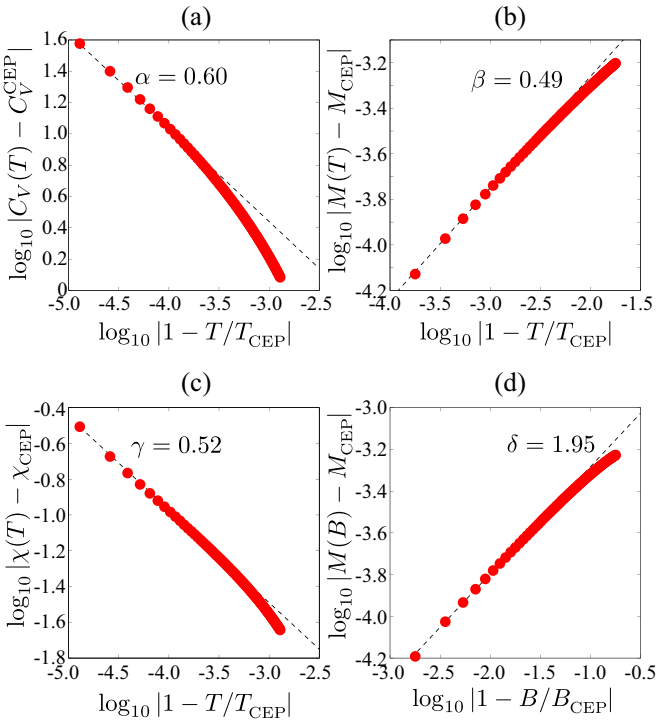

FIG. 5. Scaling behavior of $C_V(T, B)$, $M(T, B)$, and $\chi(T, B)$ around the CEP $(T_{\rm CEP}/T_c, \gamma_n B_{\rm CEP}/\pi T_c) = (0.774\,597, 0.004\,465)$. Here we use the same abbreviations as in Fig. 4.

These values agree with the values on the right-hand sides of Eqs. (1)–(3) within 10% numerical error of the exact values.

In Table I we summarize the values of the critical exponents from the BdG equation with different values of $G_0^{(n)}$ and the ones from the GL equation. Interestingly, we observe that they are close to each other, even though the positions of the CEPs on the T-B plane are different (cf. Fig. 1). The coincidence between the two suggests that the GL equation up to the eighth-order term (δ_0 term) captures the essence of the CEP of the neutron $^3P_2$ superfluid. Thus, the GL equation also supports a different universality class as discussed in Sec. II E.

IV. SUMMARY AND DISCUSSION

We have discussed the critical exponents at the CEP in the phase diagram of the neutron $^3P_2$ superfluidity, which can exist inside neutron stars. Adopting the BdG equation with the spin-polarization effect, we have obtained the critical exponents and have confirmed that they satisfy the universal relations, i.e., the Rushbrooke, Griffiths, and Widom equalities, which hold for the spin systems. We have argued that the set of critical exponents with large α and small γ belongs to a different universality class. Interesting features of the obtained critical exponents are the large α and small γ; the former indicates the slow cooling in the evolution of the neutron stars. We have checked that the spin-polarization effect induces the unique values of the critical exponents within 10% numerical errors. We also have investigated the critical exponents in the GL equation up to the eighth order and have confirmed that they satisfy the same universality relations, again within 10% errors. In spite of the different locations of the CEP in the phase diagram for the BdG equation and for the GL equation, we have found that the values of the critical exponents from the GL equation are properly regarded to be the same as the ones from the BdG equation, although there are still some discrepancies between the two due to the limited number of terms in the GL equation. Thus, we reach the conclusion that the GL equation up to the eighth order captures correctly the behaviors at the CEP in the neutron $^3P_2$ superfluids.

We leave comments on the Fermi liquid parameter $G_0^{(n)}$ in dense neutron matter for more advanced study in the future. Bäckman *et al.* [101] computed the Fermi liquid parameters including the spin channel and isospin channel of quasiparticle scattering processes and found that $G_0^{(n)}$ in Eq. (29) may be negligible. This result stems from the short-range property of the ρ-meson exchange interaction. It will be important to more carefully study the short-range behavior of the nucleon-nucleon interaction, which will be attributed to the quark-exchange contributions at the nucleon core, the core polarization in the nuclear medium, and so on. Another question we may consider is how the evolution of the neutron stars is influenced by the enhancement of the heat capacity, the magnetization, and the spin susceptibility at the CEP. That information will be useful to research the internal structures of the neutron stars through astrophysical observations.

Finally, we raise two issues. First, it is important to identify a key factor of strong deviation of critical exponents at the CEP from those of the mean-field theory. We mention that a multiple-superfluid phase diagram with a CEP was theoretically predicted in the superfluid ^{3}He under a magnetic field [102]. In addition, a Pauli-limited superconductor under a magnetic field or ultracold atomic gases with population imbalance also show the phase diagram with a CEP [103–106], but the ordered state is characterized by a single order parameter. A comprehensive study on universality class at the CEP in such single-component and multicomponent superfluids may give clues for understanding the origin of nontrivial critical behaviors. The second issue is the impact of order parameter fluctuations on the critical exponents. The nematic phases in $^3P_2$ superfluids are characterized by multiple components of the order parameter represented by the traceless symmetric tensor, leading to rich bosonic excitation spectra [63–75]. How bosonic fluctuations alter the critical behaviors at the CEP remains an issue for future research.

ACKNOWLEDGMENTS

The authors would like to thank Michikazu Kobayashi for useful discussion. This work was supported by the Grant-in-Aids for Scientific Research from Ministry of Education, Culture, Sports, Science (MEXT) of Japan [Grant No. JP15H05855 (KAKENHI on Innovative Areas "Topological Materials Science")] and the MEXT-supported Program for the Strategic Research Foundation at Private Universities "Topological Science" (Grant No. S1511006). This work was also supported in part by JSPS Grant-in-Aid for Scientific Research [KAKENHI Grants No. JP16K05448 (T.M.), No. 16H03984 (M.N.), No. 18H01217 (M.N.), and No. 17K05435 (S.Y.)].

[1] V. Graber, N. Andersson, and M. Hogg, Neutron stars in the laboratory, Int. J. Mod. Phys. D **26**, 1730015 (2017).

[2] G. Baym, T. Hatsuda, T. Kojo, P. D. Powell, Y. Song, and T. Takatsuka, From hadrons to quarks in neutron stars: A review, Rep. Prog. Phys. **81**, 056902 (2018).

[3] P. Demorest, T. Pennucci, S. Ransom, M. Roberts, and J. Hessels, Shapiro delay measurement of a two solar mass neutron star, Nature (London) **467**, 1081 (2010).

[4] J. Antoniadis, P. C. C. Freire, N. Wex, T. M. Tauris, R. S. Lynch, M. H. van Kerkwijk, M. Kramer, C. Bassa, V. S. Dhillon, T. Driebe *et al.*, A massive pulsar in a compact relativistic binary, Science **340**, 1233232 (2013).

[5] B. Abbott *et al.* (LIGO Scientific Collaboration and Virgo Collaboration), GW170817: Observation of Gravitational Waves from a Binary Neutron Star Inspiral, Phys. Rev. Lett. **119**, 161101 (2017).

[6] N. Chamel, Superfluidity and superconductivity in neutron stars, J. Astrophys. Astron. **38**, 43 (2017).

[7] B. Haskell and A. Sedrakian, Superfluidity and superconductivity in neutron stars, Astrophys. Space Sci. Libr. **457**, 401 (2018).

[8] A. Sedrakian and J. W. Clark, Superfluidity in nuclear systems and neutron stars, Eur. Phys. J. A **55**, 167 (2019).

[9] G. Baym, C. Pethick, D. Pines, and M. Ruderman, Spin up in neutron stars: The future of the Vela pulsar, Nature (London) **224**, 872 (1969).

[10] D. Pines, J. Shaham, and M. Ruderman, Corequakes and the Vela pulsar, Nat. Phys. Sci. **237**, 83 (1972).

[11] T. Takatsuka and R. Tamagaki, Corequake model of pulsar glitches for neutron stars with pion condensed core, Prog. Theor. Phys. **79**, 274 (1988).

[12] D. G. Yakovlev, A. D. Kaminker, O. Y. Gnedin, and P. Haensel, Neutrino emission from neutron stars, Phys. Rep. **354**, 1 (2001).

[13] A. Y. Potekhin, J. A. Pons, and D. Page, Neutron stars—Cooling and transport, Space Sci. Rev. **191**, 239 (2015).

[14] D. G. Yakovlev, K. P. Levenfish, and Y. A. Shibanov, Cooling neutron stars and superfluidity in their interiors, Phys. Usp. **42**, 737 (1999).

[15] C. O. Heinke and W. C. G. Ho, Direct observation of the cooling of the Cassiopeia A neutron star, Astrophys. J. Lett. **719**, L167 (2010).

[16] P. S. Shternin, D. G. Yakovlev, C. O. Heinke, W. C. G. Ho, and D. J. Patnaude, Cooling neutron star in the Cassiopeia A supernova remnant: Evidence for superfluidity in the core, Mon. Not. R. Astron. Soc. **412**, L108 (2011).

[17] D. Page, M. Prakash, J. M. Lattimer, and A. W. Steiner, Rapid Cooling of the Neutron Star in Cassiopeia A Triggered by Neutron Superfluidity in Dense Matter, Phys. Rev. Lett. **106**, 081101 (2011).

[18] P. E. Reichley and G. S. Downs, Second decrease in the period of the Vela pulsar, Nat. Phys. Sci. **234**, 48 (1971).

[19] P. W. Anderson and N. Itoh, Pulsar glitches and restlessness as a hard superfluidity phenomenon, Nature (London) **256**, 25 (1975).

[20] A. B. Migdal, Superfluidity and the moments of inertia of nuclei, Zh. Eksp. Teor. Fiz. **37**, 249 (1960) [Sov. Phys. JETP **10**, 176 (1960)].

[21] R. A. Wolf, Some effects of the strong interactions on the properties of neutron-star matter, Astrophys. J. **145**, 834 (1966).

[22] F. Tabakin, Single separable potential with attraction and repulsion, Phys. Rev. **174**, 1208 (1968).

[23] M. Hoffberg, A. E. Glassgold, R. W. Richardson, and M. Ruderman, Anisotropic Superfluidity in Neutron Star Matter, Phys. Rev. Lett. **24**, 775 (1970).

[24] R. Tamagaki, Superfluid state in neutron star matter. I: Generalized Bogoliubov transformation and existence of $^3P_2$ gap at high density, Prog. Theor. Phys. **44**, 905 (1970).

[25] T. Takatsuka and R. Tamagaki, Superfluid state in neutron star matter. II. Properties of anisotropic energy gap of $^3P_2$ pairing, Prog. Theor. Phys. **46**, 114 (1971).

[26] T. Takatsuka, Superfluid state in neutron star matter. III: Tensor coupling effect in $^3P_2$ energy gap, Prog. Theor. Phys. **47**, 1062 (1972).

[27] T. Fujita and T. Tsuneto, The Ginzburg-Landau equation for $^3P_2$ pairing: Superfluidity in neutron stars, Prog. Theor. Phys. **48**, 766 (1972).

[28] R. W. Richardson, Ginzburg-Landau theory of anisotropic superfluid neutron-star matter, Phys. Rev. D **5**, 1883 (1972).

[29] L. Amundsen and E. Østgaard, Superfluidity of neutron matter: (II). Triplet pairing, Nucl. Phys. A **442**, 163 (1985).

[30] T. Takatsuka and R. Tamagaki, Superfluidity in neutron star matter and symmetric nuclear matter, Prog. Theor. Phys. Suppl. **112**, 27 (1993).

[31] J. A. Sauls, in *Timing Neutron Stars*, edited by H. Ögelman and E. P. J. van den Heuvel, NATO Advanced Studies Institute, Series C: Mathematical and Physical Sciences (Springer, Dordrecht, 1989), Vol. 262, pp. 457–490.

[32] M. Baldo, J. Cugnon, A. Lejeune, and U. Lombardo, Proton and neutron superfluidity in neutron star matter, Nucl. Phys. A **536**, 349 (1992).

[33] Ø. Elgarøy, L. Engvik, M. Hjorth-Jensen, and E. Osnes, Triplet pairing of neutrons in β-stable neutron star matter, Nucl. Phys. A **607**, 425 (1996).

[34] V. A. Khodel, V. V. Khodel, and J. W. Clark, Universalities of Triplet Pairing in Neutron Matter, Phys. Rev. Lett. **81**, 3828 (1998).

[35] M. Baldo, Ø. Elgarøy, L. Engvik, M. Hjorth-Jensen, and H. J. Schulze, $^3P_2$–$^3F_2$ pairing in neutron matter with modern nucleon-nucleon potentials, Phys. Rev. C **58**, 1921 (1998).

[36] V. V. Khodel, V. A. Khodel, and J. W. Clark, Triplet pairing in neutron matter, Nucl. Phys. A **679**, 827 (2001).

[37] M. V. Zverev, J. W. Clark, and V. A. Khodel, $^3\mathrm{P}_2$–$^3\mathrm{F}_2$ pairing in dense neutron matter: The spectrum of solutions, Nucl. Phys. A **720**, 20 (2003).

[38] S. Maurizio, J. W. Holt, and P. Finelli, Nuclear pairing from microscopic forces: Singlet channels and higher-partial waves, Phys. Rev. C **90**, 044003 (2014).

[39] S. K. Bogner, R. J. Furnstahl, and A. Schwenk, From low-momentum interactions to nuclear structure, Prog. Part. Nucl. Phys. **65**, 94 (2010).

[40] S. Srinivas and S. Ramanan, Triplet pairing in pure neutron matter, Phys. Rev. C **94**, 064303 (2016).

[41] D. J. Dean and M. Hjorth-Jensen, Pairing in nuclear systems: From neutron stars to finite nuclei, Rev. Mod. Phys. **75**, 607 (2003).

[42] D. H. Brownell and J. Callaway, Ferromagnetic transition in superdense matter and neutron stars, Nuovo Cimento B **60**, 169 (1969).

[43] M. Rice, The hard-sphere Fermi gas and ferromagnetism in neutron stars, Phys. Lett. A **29**, 637 (1969).

[44] S. D. Silverstein, Criteria for Ferromagnetism in Dense Neutron Fermi Liquids-Neutron Stars, Phys. Rev. Lett. **23**, 139 (1969).

[45] P. Haensel and S. Bonazzola, Ferromagnetism of dense matter and magnetic properties of neutron stars, Astron. Astrophys. **314**, 1017 (1996).

[46] M. Eto, K. Hashimoto, and T. Hatsuda, Ferromagnetic neutron stars: axial anomaly, dense neutron matter, and pionic wall, Phys. Rev. D **88**, 081701(R) (2013).

[47] K. Hashimoto, Possibility of ferromagnetic neutron matter, Phys. Rev. D **91**, 085013 (2015).

[48] T. Tatsumi, Ferromagnetism of quark liquid, Phys. Lett. B **489**, 280 (2000).

[49] E. Nakano, T. Maruyama, and T. Tatsumi, Spin polarization and color superconductivity in quark matter, Phys. Rev. D **68**, 105001 (2003).

[50] K. Ohnishi, M. Oka, and S. Yasui, Possible ferromagnetism in the large N_c and N_f limit of quark matter, Phys. Rev. D **76**, 097501 (2007).

[51] G. H. Bordbar and M. Bigdeli, Spin polarized asymmetric nuclear matter and neutron star matter within the lowest order constrained variational method, Phys. Rev. C **77**, 015805 (2008).

[52] D. Blaschke, H. Grigorian, D. N. Voskresensky, and F. Weber, Cooling of the neutron star in Cassiopeia A, Phys. Rev. C **85**, 022802(R) (2012).

[53] D. Blaschke, H. Grigorian, and D. N. Voskresensky, Nuclear medium cooling scenario in light of new Cas A cooling data and the $2M_\odot$ pulsar mass measurements, Phys. Rev. C **88**, 065805 (2013).

[54] H. Grigorian, D. N. Voskresensky, and D. Blaschke, Influence of the stiffness of the equation of state and in-medium effects on the cooling of compact stars, Eur. Phys. J. A **52**, 67 (2016).

[55] J. A. Sauls and J. W. Serene, $^3P_2$ pairing near the transition temperature in neutron-star matter, Phys. Rev. D **17**, 1524 (1978).

[56] P. Muzikar, J. A. Sauls, and J. W. Serene, $^3P_2$ pairing in neutron star matter: Magnetic field effects and vortices, Phys. Rev. D **21**, 1494 (1980).

[57] J. A. Sauls, D. L. Stein, and J. W. Serene, Magnetic vortices in a rotating $^3P_2$ neutron superfluid, Phys. Rev. D **25**, 967 (1982).

[58] V. Z. Vulovic and J. A. Sauls, Influence of strong-coupling corrections on the equilibrium phase for $^3P_2$ superfluid neutron star matter, Phys. Rev. D **29**, 2705 (1984).

[59] K. Masuda and M. Nitta, Magnetic properties of quantized vortices in neutron $^3P_2$ superfluids in neutron stars, Phys. Rev. C **93**, 035804 (2016).

[60] K. Masuda and M. Nitta, Half-quantized non-Abelian vortices in neutron $^3P_2$ superfluids inside magnetars, Prog. Theor. Exp. Phys. **2020**, 013D01 (2020).

[61] T. Mizushima, K. Masuda, and M. Nitta, $^3P_2$ superfluids are topological, Phys. Rev. B **95**, 140503(R) (2017).

[62] T. Mizushima and M. Nitta, Topology and symmetry of surface Majorana arcs in cyclic superconductors, Phys. Rev. B **97**, 024506 (2018).

[63] P. F. Bedaque, G. Rupak, and M. J. Savage, Goldstone bosons in the $^3P_2$ superfluid phase of neutron matter and neutrino emission, Phys. Rev. C **68**, 065802 (2003).

[64] L. B. Leinson, New eigen-mode of spin oscillations in the triplet superfluid condensate in neutron stars, Phys. Lett. B **702**, 422 (2011).

[65] L. B. Leinson, Collective modes of the order parameter in a triplet superfluid neutron liquid, Phys. Rev. C **85**, 065502 (2012).

[66] L. B. Leinson, Neutrino emissivity of anisotropic neutron superfluids, Phys. Rev. C **87**, 025501 (2013).

[67] P. F. Bedaque and A. N. Nicholson, Low lying modes of triplet-condensed neutron matter and their effective theory, Phys. Rev. C **87**, 055807 (2013); Erratum: Low lying modes of triplet-condensed neutron matter and their effective theory [Phys. Rev. C **87**, 055807 (2013)], **89**, 029902(E) (2014).

[68] P. Bedaque and S. Sen, Neutrino emissivity from Goldstone boson decay in magnetized neutron matter, Phys. Rev. C **89**, 035808 (2014).

[69] P. F. Bedaque and S. Reddy, Goldstone modes in the neutron star core, Phys. Lett. B **735**, 340 (2014).

[70] P. F. Bedaque, A. N. Nicholson, and S. Sen, Massive and massless modes of the triplet phase of neutron matter, Phys. Rev. C **92**, 035809 (2015).

[71] L. B. Leinson, Neutrino emission from triplet pairing of neutrons in neutron stars, Phys. Rev. C **81**, 025501 (2010).

[72] L. B. Leinson, Neutrino emission from spin waves in neutron spin-triplet superfluid, Phys. Lett. B **689**, 60 (2010).

[73] L. B. Leinson, Superfluid phases of triplet pairing and neutrino emission from neutron stars, Phys. Rev. C **82**, 065503 (2010); Erratum: Superfluid phases of triplet pairing and neutrino emission from neutron stars [Phys. Rev. C **82**, 065503 (2010)], **84**, 049901(E) (2011).

[74] L. B. Leinson, Zero sound in triplet-correlated superfluid neutron matter, Phys. Rev. C **83**, 055803 (2011).

[75] L. B. Leinson, Neutrino emissivity of $^3P_2$-$^3F_2$ superfluid cores in neutron stars, Phys. Rev. C **84**, 045501 (2011).

[76] K. M. Shahabasyan and M. K. Shahabasyan, Vortex structure of neutron stars with triplet neutron superfluidity, Astrophysics **54**, 429 (2011) [Astrofizika **54**, 483 (2011)].

[77] Y. Masaki, T. Mizushima, and M. Nitta, Microscopic description of axisymmetric vortices in $^3P_2$ superfluids, Phys. Rev. Research **2**, 013193 (2020).

[78] C. Chatterjee, M. Haberichter, and M. Nitta, Collective excitations of a quantized vortex in $^3P_2$ superfluids in neutron stars, Phys. Rev. C **96**, 055807 (2017).

[79] S. Yasui and M. Nitta, Domain walls in neutron $^3P_2$ superfluids in neutron stars, Phys. Rev. C **101**, 015207 (2020).

[80] S. Yasui, C. Chatterjee, and M. Nitta, Symmetry and topology of the boundary of neutron $^3P_2$ superfluids in neutron stars: Boojums as surface topological defects, arXiv:1905.13666 [Phys. Rev. C (to be published)].

[81] N. D. Mermin, d-wave pairing near the transition temperature, Phys. Rev. A **9**, 868 (1974).

[82] D. Vollhardt and P. Wölfle, *The Superfluid Phases of Helium 3* (Dover, New York, 2013).

[83] G. E. Volovik, *The Universe in a Helium Droplet* (Clarendon, Oxford, 2003).

[84] T. Mizushima, Y. Tsutsumi, T. Kawakami, M. Sato, M. Ichioka, and K. Machida, Symmetry-protected topological

superfluids and superconductors —From the basics to ^{3}He—, J. Phys. Soc. Jpn. **85**, 022001 (2016).

[85] A. P. Mackenzie and Y. Maeno, The superconductivity of Sr_2RuO_4 and the physics of spin-triplet pairing, Rev. Mod. Phys. **75**, 657 (2003).

[86] Y. Maeno, S. Kittaka, T. Nomura, S. Yonezawa, and K. Ishida, Evaluation of spin-triplet superconductivity in Sr_2RuO_4, J. Phys. Soc. Jpn. **81**, 011009 (2012).

[87] D. Aoki, K. Ishida, and J. Flouquet, Review of U-based ferromagnetic superconductors: Comparison between UGe_2, URhGe, and UCoGe, J. Phys. Soc. Jpn. **88**, 022001 (2019).

[88] Y. Kawaguchi and M. Ueda, Spinor Bose-Einstein condensates, Phys. Rep. **520**, 253 (2012).

[89] S. Yasui, C. Chatterjee, and M. Nitta, Phase structure of neutron $^3P_2$ superfluids in strong magnetic fields in neutron stars, Phys. Rev. C **99**, 035213 (2019).

[90] S. Yasui, C. Chatterjee, and M. Nitta, Effects of strong magnetic fields on neutron $^3P_2$ superfluidity in spin-orbit interactions, JPS Conf. Proc. **26**, 024022 (2019).

[91] S. Yasui, C. Chatterjee, M. Kobayashi, and M. Nitta, Revisiting Ginzburg-Landau theory for neutron $^3P_2$ superfluidity in neutron stars, Phys. Rev. C **100**, 025204 (2019).

[92] S. Uchino, M. Kobayashi, M. Nitta, and M. Ueda, Quasi-Nambu-Goldstone Modes in Bose-Einstein Condensates, Phys. Rev. Lett. **105**, 230406 (2010).

[93] P. M. Chaikin and T. C. Lubensky, *Principles of Condensed Matter Physics* (Cambridge University Press, Cambridge, 1995).

[94] J. Zinn-Justin, *Quantum Field Theory and Critical Phenomena* (Clarendon, Oxford, 2002).

[95] R. Guida and J. Zinn-Justin, 3D Ising model: The scaling equation of state, Nucl. Phys. B **489**, 626 (1997).

[96] S. Yin, S.-K. Jian, and H. Yao, Chiral Tricritical Point: A New Universality Class in Dirac Systems, Phys. Rev. Lett. **120**, 215702 (2018).

[97] J. Serene and D. Rainer, The quasiclassical approach to superfluid ^{3}He, Phys. Rep. **101**, 221 (1983).

[98] J. A. Sauls, in *Strongly Correlated Electronic Materials—The Los Alamos Symposium 1993*, edited by K. Bedell, Z. Wang, D. Meltzer, A. Balatsky, and E. Abrahams (Addison-Wesley, New York, 1994).

[99] A. B. Vorontsov and J. A. Sauls, Thermodynamic properties of thin films of superfluid ^{3}He-*A*, Phys. Rev. B **68**, 064508 (2003).

[100] T. Mizushima, Superfluid ^{3}He in a restricted geometry with a perpendicular magnetic field, Phys. Rev. B **86**, 094518 (2012).

[101] S.-O. Bäckman, G. E. Brown, and J. A. Niskanen, The nucleon-nucleon interaction and the nuclear many-body problem, Phys. Rep. **124**, 1 (1985).

[102] M. Ashida and K. Nagai, *A*-*B* transition of superfluid ^{3}He under magnetic field at low pressures, Prog. Theor. Phys. **74**, 949 (1985).

[103] K. Machida, T. Mizushima, and M. Ichioka, Generic Phase Diagram of Fermion Superfluids with Population Imbalance, Phys. Rev. Lett. **97**, 120407 (2006).

[104] T. Mizushima, M. Takahashi, and K. Machida, Fulde-Ferrell-Larkin-Ovchinnikov states in two-band superconductors, J. Phys. Soc. Jpn. **83**, 023703 (2014).

[105] L. Radzihovsky and D. E. Sheehy, Imbalanced Feshbach-resonant Fermi gases, Rep. Prog. Phys. **73**, 076501 (2010).

[106] J. J. Kinnunen, J. E. Baarsma, J.-P. Martikainen, and P. Törmä, The Fulde-Ferrell-Larkin-Ovchinnikov state for ultracold fermions in lattice and harmonic potentials: A review, Rep. Prog. Phys. **81**, 046401 (2018).